Biogeosciences Discuss., https://doi.org/10.5194/bg-2017-471
Manuscript under review for journal Biogeosciences
Discussion started: 8 November 2017
© Author(s) 2017. CC BY 4.0 License.

The triple oxygen isotope composition of phytoliths as a proxy of continental atmospheric humidity: insights from climate chamber and climate transect calibrations

Anne Alexandre[1], Amaelle Landais[2], Christine Vallet-Coulomb[1], Clément Piel[3], Sébastien Devidal[3], Sandrine Pauchet[1], Corinne Sonzogni[1], Martine Couapel[1], Marine Pasturel[1], Pauline Cornuault[1], Jingming Xin[2], Jean-Charles Mazur[1], Frédéric Prié[2], Ilhem Bentaleb[4], Elizabeth Webb[5], Françoise Chalié[1], Jacques Roy[3].

[1] CEREGE UM34, Aix-Marseille Université, CNRS, IRD, INRA, Aix en Provence, France
[2] Laboratoire des Sciences du Climat et de l'Environnement (LSCE/IPSL/CEA/CNRS/UVSQ), Gif-sur-Yvette, France
[3]Ecotron Européen de Montpellier, UPS 3248, Centre National de la Recherche Scientifique (CNRS), Campus Baillarguet, Montferrier-sur-Lez, France
[4] ISEM, Université de Montpellier, CNRS, IRD, EPHE, Montpellier, France
[5]Department of Earth Sciences, The University of Western Ontario, London, Ontario,Canada

Correspondance: alexandre@cerege.fr

Abstract

Continental atmospheric relative humidity (RH) is a key climate-parameter. Combined with atmospheric temperature, it allows us to estimate the concentration of atmospheric water vapor which is one of the main components of the global water cycle and the most important gas contributing to the natural greenhouse effect. However, there is a lack of proxies suitable for reconstructing, in a quantitative way, past changes of continental atmospheric humidity. This reduces the possibility to make model-data comparisons necessary for the implementation of climate models. Over the past 10 years, analytical developments have enabled a few laboratories to reach sufficient precision for measuring the triple oxygen isotopes, expressed by the ^{17}O-excess (^{17}O-excess = ln (δ^{17}O + 1) – 0.528 x ln (δ^{18}O + 1)), in water, water vapor and minerals. The ^{17}O-excess represents an alternative to deuterium-excess for investigating relative humidity conditions that prevail during water evaporation. Phytoliths are micrometric amorphous silica particles that form continuously in living plants. Phytolith morphological assemblages from soils and sediments are commonly used as past vegetation and hydrous stress indicators. In the present study, we examine whether changes in atmospheric RH imprint the ^{17}O-excess of phytoliths in a measurable way and whether this imprint offers a potential for reconstructing past RH. For that purpose, we first monitored the ^{17}O-excess evolution of soil water, grass leaf water and grass phytoliths in response to changes in RH (from 40 to 100 %) in a growth chamber experiment where transpiration reached a steady state. Decreasing RH decreases the ^{17}O-excess of phytoliths by 4.1 per meg / % as a result of kinetic fractionation of the leaf water subject to evaporation. In order to model with accuracy the triple oxygen isotope fractionation in play in plant water and in phytoliths we recommend direct and continuous measurements of the triple isotope composition of water vapor. Then, we measured the ^{17}O-excess of 57 phytolith assemblages collected from top soils along a

Biogeosciences Discuss., https://doi.org/10.5194/bg-2017-471
Manuscript under review for journal Biogeosciences
Discussion started: 8 November 2017
© Author(s) 2017. CC BY 4.0 License.

RH and vegetation transect in inter-tropical West and Central Africa. Although scattered, the ^{17}O-excess of phytoliths decreases with RH by 3.4 per meg / %. The similarity of the trends observed in the growth chamber and nature supports that RH is an important control of ^{17}O-excess of phytoliths in the natural environment. However, other parameters such as changes in the triple isotope composition of the soil water or phytolith origin in the leaf tissue may come into play. Assessment of these parameters through additional growth chambers experiments and field campaigns will bring us closer to an accurate proxy of changes in relative humidity.

1 Introduction

Continental atmospheric relative humidity (RH) is a key climate-parameter. Combined with atmospheric temperature, it allows scientists to estimate the concentration of atmospheric water vapor which is one of the main components of the global water cycle and the most important gas contributing to the natural greenhouse effect (e.g. Held and Soden, 2000; Dessler and Davis, 2010; Chung et al., 2014). However, global climate models (GCMs) have difficulties to properly capture continental humidity conditions (Sherwood et al., 2010; Risi et al., 2012; Fischer and Knutti, 2013). Although tropospheric RH results from a subtle balance between different processes (including air mass origins and trajectories, large scale radiative subsidence, evaporation of falling precipitation, detrainment of convective system, evapotranspiration), it is usually depicted as rather constant in GCMs in agreement with thermodynamic coupling between atmospheric water vapor and sea surface temperature (Bony et al., 2006). A model-data comparison approach is thus essential to progress on this issue. This approach has to be applicable beyond the instrumental period to make use of past changes in atmospheric water vapor conditions.

There are multiple ways to reconstruct past continental temperature and precipitation, for instance from pollen (Bartlein et al., 2010; Herbert and Harrison, 2016; Wahl et al., 2012) or tree ring data (Labuhn et al., 2016; Lavergne et al., 2017). However, there is a serious lack of proxies suitable for reconstructing, in a quantitative way, past variations in continental atmospheric RH. Indeed, the stable isotopes of oxygen and hydrogen (δ^{18}O and δD) of tree rings can be influenced by several parameters other than humidity (precipitation source, temperature). This limits the interpretation of tree ring isotope series in terms of humidity changes to places where variations of these other parameters are well constrained (Grießinger et al., 2016; Wernicke et al., 2015). A promising method relies on the δ^{18}O and δD of plant biomarkers (e.g. n-alkanes and fatty acids from leaf waxes) recovered from soils (or buried soils) and sediments. It allows for an estimate in changes in plant water deuterium-excess (d-excess = δD - 8.0 x δ^{18}O), linked to changes in precipitation sources and RH. This method under development can however be biased by factors other than climatic such as plant functional types and selective degradation of the biomarkers (e.g. Schwab et al., 2015; Tuthorn et al., 2015).

Phytoliths are micrometric amorphous silica (SiO_2, nH_2O) particles that form continuously in living plants. Silicon is actively absorbed by the roots (Ma and Yamaji, 2006) and is translocated in the plant tissues where it polymerizes inside the cells, in the cell walls and in extracellular spaces

Biogeosciences Discuss., https://doi.org/10.5194/bg-2017-471
Manuscript under review for journal Biogeosciences
Discussion started: 8 November 2017
© Author(s) 2017. CC BY 4.0 License.

of stems and leaves. Silica polymerization appears to be an active physiological process, which does not only depends on transpiration (Kumar et al., 2017). In grasses, which are well known silica accumulators, silica accounts for several % of dry weight (d.w.) and is mainly located in the stem and leaf epidermis. Phytolith morphological assemblages from soils and sediments are commonly used as past vegetation and hydrous stress indicators (e.g. Aleman et al., 2012; Backwell et al., 2014; Bremond et al., 2005a, 2005b; Contreras et al., 2014; Nogué et al., 2017 ; Piperno, 2006). The potential of the $\delta^{18}O$ signature of phytoliths ($\delta^{18}O_{Phyto}$) from grasses for paleoclimate reconstruction has been investigated through growth chamber and North American Great Plains calibrations. It has been shown that the $\delta^{18}O_{Phyto}$ of grass stems weakly affected by transpiration correlated with the $\delta^{18}O$ signature of soil water ($\delta^{18}O_{SW}$) and the atmospheric temperature, as expected for a polymerization of silica in isotope equilibrium with the plant water (Webb and Longstaffe, 2000, 2002, 2003, 2006). This was not the case for $\delta^{18}O_{Phyto}$ from grass leaves that correlated with RH as expected for an evaporative kinetic isotope enrichment of the leaf water (e.g. Cernusak et al., 2016) imprinted on $\delta^{18}O_{Phyto}$. However, because grass stem and leaf phytoliths have the same morphology and are mixed in soil and sedimentary samples, these calibrations were not sufficient for using $\delta^{18}O_{Phyto}$ of grassland phytolith assemblages as a paleoclimatic signal. In tropical trees, silica is found in leaves, bark and wood and accounts for a few % d.w. (e.g. Collura and Neumann, 2017). In the wood, silica polymerizes in the secondary xylem supposedly unaffected by transpiration, in the form of Globular granulate phytolith types (Madella et al., 2005; Scurfield et al., 1974; Welle, 1976). These phytoliths make up more than 80% of tropical humid forest and rainforest phytolith assemblages found in soils and sediments (Alexandre et al., 2013; Collura and Neumann, 2017; Scurfield et al., 1974; Welle, 1976). Examination of the $\delta^{18}O_{Phyto}$ of rainforest assemblages showed correlations with the $\delta^{18}O$ of precipitation ($\delta^{18}O_{Pre}$) and the atmospheric temperature (Alexandre et al., 2012). However, in this case, the use of $\delta^{18}O_{Phyto}$ did not further develop because it was applicable only to forested areas and humid climatic periods, which is a major drawback for paleoclimatic reconstructions.

The triple isotope composition of oxygen in the water molecule represents an alternative for investigating RH conditions prevailing during water evaporation. In the triple isotope system, the mass-dependent fractionation factors between A and B ($^{17}\alpha_{A-B}$ and $^{18}\alpha_{A-B}$) are related by the exponent θ_{A-B} ($^{17}\alpha_{A-B} = {}^{18}\alpha_{A-B}{}^{\theta}$ or $\theta_{A-B} = \ln {}^{17}\alpha_{A-B} / \ln {}^{18}\alpha_{A-B}$). In delta notation, the relationship becomes $\theta_{A-B} = \ln(1 + \Delta^{17}_{A-B}) / \ln(1 + \Delta^{18}_{A-B})$, where $\Delta^{*}_{A-B} = ({}^{*}\delta_a - {}^{*}\delta_b) / ({}^{*}\delta_b + 1)$ is expressed in ‰. * denotes 17 or 18. This expression of Δ^{*}_{A-B} is more accurate than its linearized form ($\Delta^{*}_{A-B} = \delta^{*}_{A} - \delta^{*}_{B}$) (Angert et al., 2003; Miller, 2002). It has been recently empirically estimated that θ equals 0.529 for liquid-vapor equilibrium (θ_{equil}; Barkan and Luz, 2005) and 0.518 for vapor diffusion in air (Barkan and Luz, 2007). The triple oxygen isotope composition can also be described graphically in a $\ln(\delta^{17}O + 1)$ *vs* $\ln(\delta^{18}O + 1)$ space, in which θ represents the slope of the data alignment during a mass-dependent fractionation process. The ln expression of $\delta^{17}O$ and $\delta^{18}O$ are referred to as $\delta'^{17}O$ and $\delta'^{18}O$. In this space, meteoric waters plot along a line with a slope θ of

© Author(s) 2017. CC BY 4.0 License.

117 0.528 ± 0.001. The departure from the meteoric water line is conventionally called ^{17}O-excess (^{17}O-
118 excess = $\delta'^{17}O - 0.528 \times \delta'^{18}O$) (Luz and Barkan, 2010). In case of mass-dependent fractionation
119 processes, the magnitudes of the ^{17}O-excess in waters and minerals are very small and
120 measurement of the ^{17}O-excess, expressed in per meg (10^{-3} ‰) *vs* VSMOW, requires to reach very
121 high analytical precisions.

122 In the water cycle, the ^{17}O-excess variations mainly result from diffusion processes, while
123 equilibrium fractionation does not lead to important departure from the meteoric water line.
124 Theoretical and empirical estimations have shown that in contrast to d-excess, and except at very
125 high latitudes, changes in water ^{17}O-excess are not significantly impacted by temperature (~0.1 per
126 meg / °C ; Uemura et al., 2010) and much less sensitive to distillation processes (Angert et al.,
127 2004; Barkan and Luz, 2007; Landais et al., 2008; Uemura et al., 2010; Steig et al., 2014). Changes
128 in water ^{17}O-excess are thus essentially controlled by evaporative kinetic fractionation. The ^{17}O-
129 excess decreases in the evaporating water and increases in the vapor phase when RH decreases at
130 evaporative sites (e.g. sea surface, lake surface, soil surface or leaf surface). Over the last ten
131 years, a few studies used the ^{17}O-excess of water to interpret ice core archives in climatic terms
132 (Guillevic et al., 2014, Schoeneman et al., 2014; Winkler et al., 2012; Landais et al., 2008, 2012).
133 They supported that ^{17}O-excess is a marker of RH, sea-ice extent at the moisture source, and air
134 mass mixing (Risi et al., 2010) except at the very high latitudes of East Antarctica where
135 temperature can have a significant influence. The observed variations of ^{17}O-excess in Greenland
136 ice cores of ~20 per meg maximum were thus interpreted as variations of RH or sea-ice extent at
137 the source region and coincide with variations in the low to mid latitude water cycle as recorded
138 by other proxies (such as CH_4 or δD of CH_4) (Guillevic et al., 2014). An even smaller number of
139 studies measured or attempted to model the ^{17}O-excess of rainwater at low and temperate latitudes
140 (Affolter et al., 2015; Landais et al., 2010b; Li et al., 2015; Luz and Barkan, 2010; Risi et al.,
141 2013). The observed variations in ^{17}O-excess, partly explained by convective processes and re-
142 evaporation of precipitation, were of the order of 30-40 per meg, either during a rainy event or
143 along climatic gradients. Only two studies focused on open surface waters, and showed that
144 variations of the ^{17}O-excess ranged from tens to hundreds of per meg when the surface water
145 underwent strong evaporative enrichment (Surma et al., 2015; Luz and Barkan, 2010), in
146 agreement with the Craig and Gordon (1965) formulation. The most important variations in ^{17}O-
147 excess occur at the plant-atmosphere interface. In leaf water, variations higher than 200 per meg
148 were encountered (Landais et al., 2006; Li et al., 2017). Difference in ^{17}O-excess between leaf
149 water subject to evaporation (LW) and stem water (SW) not subject to evaporation, increased with
150 decreasing RH (from 100 to 30 %), as expected for processes dominated by kinetic fractionation.
151 When measuring a sequence of LW- SW couples sampled under different climatic conditions, the
152 slope of the line linking their triple isotope composition and named λ_{transp}, equivalent to $\theta_{LW\text{-}SW}$, was
153 found to change with RH. This pattern was neither influenced by the plant species nor by the
154 environmental conditions (e.g. atmospheric temperature, soil water conditions) (Landais et al.,
155 2006). However opposite trends of λ_{transp} with RH were observed from one study to another

Biogeosciences Discuss., https://doi.org/10.5194/bg-2017-471
Manuscript under review for journal Biogeosciences
Discussion started: 8 November 2017
© Author(s) 2017. CC BY 4.0 License.

(Landais et al., 2006; Li et al., 2017). This discrepancy was attributed to the possibility that steady state is not always reached during sampling and to likely differences in isotope composition of the ambient vapor, a parameter of the Craig and Gordon model that is often not measured but estimated (Li et al., 2017).

While ^{17}O-excess measurements of waters were expanding, analyses of the triple oxygen isotope composition of minerals (mostly silicates and carbonates) were also developed, allowing estimate of fractionation during polymerization and providing constraints on both temperature and isotope composition of the water source (Pack and Herwartz, 2014; Levin et al., 2014; Passey et al., 2014; Herwartz et al., 2015; Miller et al., 2015; Sharp et al., 2016). Variations of ^{17}O-excess of the order of tens to hundreds of per meg were reported from one mineral to another. For most of the studies cited above, the objective was to discriminate between high and low temperature formation processes or to decipher from which type of water the mineral formed (i.e. sea water, hydrothermal water, meteoric or surface water). The ^{17}O-excess of biogenic and sedimentary carbonates was also investigated as a potential record of evaporating water sources (Passey et al., 2014).With regard to silicate-water fractionation, the relationship between the three oxygen isotopes defined by $\theta_{SiO2\text{-}water}$ was estimated between 0.521 and 0.528, increasing logarithmically with temperature (Sharp et al., 2016).

In the present study, in the light of the recent findings cited above, we examined whether changes in atmospheric RH imprint the ^{17}O-excess of phytoliths (^{17}O-excess$_{Phyto}$) in a measurable way and whether this imprint offers a potential for reconstructing past RH. For that purpose, we first monitored the ^{17}O-excess evolution of soil water, grass leaf water and grass phytoliths in response to changes in RH in a growth chamber experiment. Then, we measured the ^{17}O-excess$_{Phyto}$ from 57 phytolith assemblages collected in soil tops along a RH and vegetation transect in inter-tropical West and Central Africa. Relationships between ^{17}O-excess$_{Phyto}$ and RH were looked for and assessed on the basis of previous quantifications of kinetic isotope enrichment of leaf water and equilibrium fractionation between water and silica. Results from the natural sampling were compared to the ones from the growth chamber experiment to evaluate the importance of RH in controlling ^{17}O-excess$_{Phyto}$ in natural environment.

2 Materials and methods

2.1 Samples from the growth chamber experiment

Festuca arundinacea, commonly referred to as tall fescue, is widely distributed globally as a forage and an invasive grass species (Gibson and Newman, 2001) and can adapt to a wide range of conditions. In 2016, *F. arundinacea* (Callina RAGT Semences) was grown in three chambers under three conditions of RH (ca. 40, 60 and 80 %) kept constant using wet air introduction and ultrasonic humidifier. We checked that the humidifiers did not lead to any isotope fractionation between the water in their reservoirs and the vapor delivered. Temperature and light intensity were kept constant at 25 ± 0.6 (SD) °C and 293 ± 14 (SD) mmol / m^2 / sec respectively.

In a 35 L tank (53 x 35 x 22 cm), 20 kg of dried commercial potting soil were packed above a 1.6

© Author(s) 2017. CC BY 4.0 License.

cm layer of quartz gravel. A porous cup for water extraction was placed in the soil with its extraction tube hermetically extending outside of the tank walls. The soil was irrigated with 10 L of the same water as the one used for the humidifier. Four grams of seeds were sown along four rows in each tank, resulting in about 6000 seedlings. Each tank was then placed in a chamber and was irrigated from a Mariotte bottle (25 L) placed next to it. The Mariotte system was set so that a water saturated level of 5 cm remained constant at the base of the tank. The irrigation water was supplemented with 105 mg/L of SiO_2 (in the form of SiO_2 K_2O). Ten days after germination, agar-agar (polysaccharide agarose) was spread on the soil surface around the seedlings (about 8 cm tall), to prevent any evaporation (Alexandre et al., 2016).

A fourth tank was kept at 100% of RH thanks to the installation of a 20 cm high plexiglass cover, in a forth chamber set at 80 % of RH. In this case no agar-agar was added and the vapor around *F. arundinacea* came from evaporation and transpiration of the soil water. Otherwise the treatment was the same as in the other chambers.

For each humidity condition, three to four harvests were made at intervals of 10-14 days. The 20-25 cm long leaves were cut at two cm above the soil level and weighed. From the first to the fourth sampling, the harvested wet leaves increased from 15-20 g (10 days of growth) to 40-60 g (14 days of growth). Three to five g of leaves were put in glass gastight vials and kept frozen for bulk leaf water extraction. The remaining leaves were dried for phytolith extraction. Forty mL of irrigation water from the Mariotte bottle, and of soil water from the porous cup, were kept at 5°C before analyses.

After each harvest, the tanks were left in their chamber of origin but the 40, 60 and 80 % RH treatments were rotated between the growth chambers so that the four replicates of a given RH treatment would come from at least two different chambers. The 100 % humidity was set up in a unique chamber during the entire duration of the experiment. The harvested leaves in this treatment were often covered by condensation drops which were blotted between two sheets of wiping paper, rapidly after harvesting. The experimental setup details and the harvest list are given in table 1.

2.2 Samples from the natural climate transects

Fifty-seven top soil samples were collected during several field trips along vegetation and humidity transects in Mauritania and Senegal (Bremond et al., 2005b ; Lézine, 1988; Pasturel, 2015) (Lezine, 1988) Gabon (Lebamba et al., 2009) and Congo (Alexandre et al., 1997) in the saharian, sahelian, sudanian, guinean and congolian bioclimatic zones, respectively (White et al., 1983). Samplings, phytolith extractions and phytolith morphological assemblages descriptions are given in the above-mentioned studies, except for the samples of Gabon from which phytoliths were chemically treated and counted in the frame of the present study.

The sampled site location as well as the associated climatic and oxygen isotope variables are given in Table 2. The vegetation overlying the sampled soils was categorized into savanna (Mauritania, Senegal), wooded savanna (Senegal), humid forest (Gabon and Congo) and enclosed savanna (Gabon). For each sampled site, yearly climate average were calculated from the monthly means

© Author(s) 2017. CC BY 4.0 License.

of temperature, precipitation, RH and diurnal temperature, extracted from the Climate Research Unit (CRU) 1961 - 1990 time series (10' spatial resolution; http://www.cru.uea.ac.uk, Harris et al., 2013, CRU 2.0). Mean Annual Precipitation (MAP), Mean Annual Temperature (MAT) and mean annual RH range from 49 to 2148 mm, 24.3 to 29.8 °C and 40.2 to 82.5 %, respectively. In addition, in order to get a proxy of RH during the grass growing season, averaged RH monthly means for months with at least one day with precipitation higher than 0.1 mm (RH-rd0>1) was calculated. It ranges from 56.3 to 82.5 %. As maximum transpiration is supposed to be reached around 15:00 UTC we also calculated RH and RH-rd0>1 at 15:00 (RH15 and RH15-rd0>1, respectively) according to New et al. (2002) and Kriticos et al. (2012). For each sampling site, estimates of $\delta^{18}O$ of precipitation for the months with at least one day with precipitation higher than 0.1 mm ($\delta^{18}O_{Pre\ rd0>1}$) were extracted from The Online Isotopes in Precipitation Calculator-version OIPC2-2 (http://www.waterisotopes.org; Bowen and Revenaugh, 2003; Bowen and Wilkinson, 2002; Bowen et al., 2005) and weighted by the amount of precipitation. The estimates range from -3.22 to -4.33 ‰. There is currently no data on the ^{17}O-excess of precipitation (^{17}O-excess$_{Pre}$) at these sites.

2.3 Phytolith chemical extractions

Phytoliths from soils were extracted following Crespin et al. (2008) using HCl, H_2O_2, $C_6H_5Na_3O_7$ and $Na_2O_4S_2$-H_2O at 70 °C, and a $ZnBr_2$ heavy liquid separation. It has been shown that up to a temperature of 70 °C the extraction has no effect on the $\delta^{18}O$ of phytoliths (Crespin et al., 2008). We verified that it did not have any effect on the ^{17}O-excess either. Phytoliths from *Festuca arundinaceae* were extracted using a high purity protocol with HCl, H_2SO_4, H_2O_2, HNO_3, $KClO_3$ and KOH at 70 °C following Corbineau et al. (2013).

2.4 Phytolith counting

Phytolith assemblages from the humidity transects were mounted on microscope slides in Canada Balsam, for counting, at a 600X magnification. More than 200 identifiable phytoliths with a diameter greater than 5 µm and with a taxonomic significance were counted per sample. Three repeated counting gave an error of ± 3.5 % (SD). Phytoliths were named using the International Code for Phytolith Nomenclature 1.0 (Madella et al., 2005) and categorized as Globular granulate type produced by the wood (Scurfield et al., 1974; Kondo et al., 1994), palm Globular echinate type and grass types comprising Acicular, Bulliform, Elongate psilate, Elongate echinate, Bulliform cells, and Grass Short Cells types. For each sample from the natural transects, the phytolith index d/p, a proxy of tree cover density (Alexandre and Bremond, 2009; Bremond et al., 2005a), was calculated. It is the ratio of Globular granular phytolith category (Madella et al., 2005) formed in the secondary xylem of the dicotyledon (d) wood to the grass short cell phytolith category formed in the epidermis of grasses or Poideae (p) (Collura and Neumann, 2017; Scurfield et al., 1974; Welle, 1976). Those two categories make up most of the phytolith assemblages recovered from inter-tropical soils (Bremond et al., 2005a, 2005b; Alexandre et al., 1997, 2013; Bremond et al., 2005b, 2005a).

Biogeosciences Discuss., https://doi.org/10.5194/bg-2017-471
Manuscript under review for journal Biogeosciences
Discussion started: 8 November 2017
© Author(s) 2017. CC BY 4.0 License.

Phytolith assemblages from the *F. arundinacea* samples were also mounted and counted. The phytolith types were categorized according to their cell of origin in the epidermis into Epidermal short cell, Epidermal long cell, Bulliform cell and Hair acicular.

2.5 Leaf and soil water extraction

Leaf water was extracted using a distillation line. Leaves were introduced in a glass tube connected to the distillation line, and frozen through immersion of the glass tube in liquid nitrogen. While keeping the sample frozen, the distillation line was pumped to reach a vacuum higher than 5.10^{-2} mbar. The pumping system was then isolated and the glass sample tube warmed to 80°C. Meanwhile, at the other end of the distillation line, a glass collecting tube was immersed in liquid nitrogen to trap the extracted water. To avoid condensation, the line between the sample tube and the collection tube was heated with a heating wire. The distillation was completed after six hours. In order to remove volatiles from the extracted water, a few granules of activated charcoal were added and the water slowly stirred for 12 h.

Soil water was extracted using a 31mm porous ceramic cup. Brown or yellow-colored samples were filtered at 0.22µm, but remain colored after filtration, indicating the presence of soluble compounds.

2.6 Isotope analyses

The oxygen isotope results are expressed in the standard δ-notation relative to VSMOW.

2.6.1 Phytoliths

Phytolith samples of 1.6 mg were dehydrated under a flow of N_2 (Chapligin et al., 2010) and oxygen extraction was performed using the IR Laser-Heating Fluorination Technique at CEREGE (Aix-en-Provence, France) (Alexandre et al., 2006, Crespin et al., 2008; Suavet et al., 2010). The purified oxygen gas (O_2) was passed through a −114 °C slush to refreeze potential gases interfering with the mass 33 (e.g. NF) before being sent to the dual-inlet mass spectrometer (ThermoQuest Finnigan Delta Plus). The composition of the reference gas was determined through the analyses of NBS28 for which isotope composition has been set to $\delta^{18}O$=9.600 ‰, $\delta^{17}O$=4.992 ‰ and ^{17}O-excess = -65 per meg. During the measurement period, reproducibility (SD) of the analyses of the working quartz standard (Boulangé 2008) against which the isotope composition of the sample gas was corrected on a daily basis (3 quartz standards were analysed per day) was ± 0.196 ‰, ± 0.106 ‰ and ± 22 per meg for $\delta^{18}O$, $\delta^{17}O$ and ^{17}O-excess respectively (n = 63; one run of eight dual inlet measurements). For every session of measurement, the effectiveness of the entire dehydration and IR-Laser-Fluorination-IRMS procedure was checked through the analysis of a working phytolith standard (MSG60) with $\delta^{18}O$ = 36.904 ± 0.781 ‰, $\delta^{17}O$ = 19.100 ± 0.405 ‰ and ^{17}O-excess = -215 ± 34 per meg (n = 29). For comparison, the inter-laboratory pooled value for MSG60 is $\delta^{18}O$ = 37.0 ± 0.8 ‰ (Chapligin et al., 2011). Recent measurements of the silicate reference materials UWG-2 garnet (Valley et al., 1995) and San Carlos (SC) olivine gave the following values: $\delta^{18}O_{UWG-2}$ = 5.724 ± 0.124 ‰, $\delta^{17}O_{UWG-2}$ = 2.950 ± 0.057 ‰, ^{17}O-excess $_{UWG-2}$ = -68 ± 27 per meg (n = 5), $\delta^{18}O_{SC}$ = 4.949 ± 0.219 ‰, $\delta^{17}O_{SC}$ = 2.561 ± 0.122 ‰, ^{17}O-excess$_{SC}$ = -49 ± 24 per meg (n

© Author(s) 2017. CC BY 4.0 License.

= 3). For comparison, silicate analyses presented in Sharp et al. (2016) are normalized to a $\delta^{18}O$ value for San Carlos Olivine of 5.3 ‰ and a ^{17}O-excess value of -54 per meg.

2.6.2 Leaf water

Leaf water was analyzed at LSCE (Gif sur Yvette, France) following the procedure previously detailed in Landais et al. (2006). In summary, a fluorination line was used to convert water to oxygen using CoF_3 heated at 370°C in a helium flow. The oxygen was then trapped in a tube immersed in liquid helium before being analyzed by dual inlet IRMS (ThermoQuest Finnigan Delta V mass spectrometer) against a reference oxygen gas. All measurements were run against a working O_2 standard calibrated against VSMOW. The resulting precisions (2 runs of 16 dual inlet measurements) were 0.02 ‰ for both $\delta^{17}O$ and $\delta^{18}O$ and 5 ppm for ^{17}O-excess.

2.6.3 Irrigation and soil waters

Irrigation and soil water were analyzed at the Ecotron of Montpellier (France) with an isotope laser analyzer (Picarro L2140i) operated in ^{17}O-excess mode using an auto-sampler and a high precision vaporizer. Each water sample was used to fill three vials randomly dispatched in four groups of six samples (three replicates per sample). Each sample group was bracketed by three working standards (Giens-1, Iceberg-1 and Eco-1). Ten injections were performed for each vial, and the results of the first six injections were discarded to account for memory effects. Following IAEA recommendations (IAEA, 2013), each liquid measurement sequence was started with two vials of deionized water for instrument conditioning.

The isotope compositions of each sample group were calibrated using the three interpolated mean values obtained for the bracketing working standards (Delattre et al., 2015). All isotope ratios were normalized on the VSMOW2/SLAP2 scale, with an assigned SLAP2 ^{17}O-excess value of zero, following the recommendations of Schoenemann et al. (2013). The resulting precisions (3 replicates) were 0.018 ‰, 0.015 ‰ and 10 per meg for $\delta^{17}O$, $\delta^{18}O$ and ^{17}O-excess (n=31).

The three working standards were also analyzed using the fluorination/IRMS technique used for leaf water analyses at LSCE. The ^{17}O-excess maximum difference was 6.4 per meg, which is lower than the analytical precision obtained using the laser spectrometer.

In order to assess that soluble organic compounds present in some soil water samples did not impact the laser analyzer isotope measurements (Martín-Gómez et al., 2015), a representative set of colored samples were analyzed with and without a Picarro micro combustion module (MCM) set up between the high precision vaporizer and the analyzer inlet. This system was designed to partly remove organic volatile compounds using a catalytic process. The obtained isotope compositions were not significantly different, suggesting that organic compounds were either in low concentration, and/or did not interfere in the spectral window used by the analyzer. Therefore, the other soil water samples were analyzed without the MCM.

3 Results

3.1 Growth chamber experiment

Biogeosciences Discuss., https://doi.org/10.5194/bg-2017-471
Manuscript under review for journal Biogeosciences
Discussion started: 8 November 2017
© Author(s) 2017. CC BY 4.0 License.

345 $\delta'^{18}O$ and ^{17}O-excess of the irrigation water (respectively $\delta'^{18}O_{IW}$ and $^{17}O\text{-excess}_{IW}$) average -
346 5.586 ± 0.006‰ and 26 ± 5 per meg, respectively. $\delta'^{18}O$ and ^{17}O-excess of the soil water
347 (respectively $\delta'^{18}O_{SW}$ and $^{17}O\text{-excess}_{SW}$) average -2.889 ± 0.188 ‰ and 16 ± 8 per meg,
348 respectively (table S1). The isotope difference is thus significant for $\delta'^{18}O$, less significant for ^{17}O-
349 excess, according to the analytical error. Although evaporative kinetic fractionation of the top soil
350 water suctioned by the porous cup under vacuum cannot be ruled out, isotopic exchanges between
351 the soil water and oxygen-bearing phases of the rhizosphere may also have impacted the soil water
352 isotopic composition (Bowling et al., 2017; Chen et al., 2016; Oerter et al., 2014; Orlowski et al.,
353 2016). Hereinafter, we consider the isotope signatures of the water absorbed by the roots of *F.*
354 *arundinacea* to be equivalent to the irrigation water that fed the saturation level at the base of the
355 tank. This water was reached by the deepest roots, as observed on a cross-section of the soil after
356 the end of the experiment and likely reached the upper roots by capillarity.

357 The transpiration of *F. arundinacea* increases linearly from 0.03 to 0.6 L / day from 100 to 60 %
358 RH and stabilizes around 0.6 L / day from 60 to 40 % RH (averages of the replicates, Table 1). In
359 response to decreasing RH, $\delta'^{18}O$ (table S1) and ^{17}O-excess (fig. 1a) values of the bulk leaf water
360 ($\delta'^{18}O_{LW}$ and $^{17}O\text{-excess}_{LW}$) show clear increasing and decreasing trends, respectively. The
361 averaged ^{18}O-enrichment of bulk leaf water relatively to irrigation water ($\Delta^{18}_{LW\text{-}IW}$) increases from
362 11.263 ± 4.987 and 7.516 ± 0.708 ‰ at 100 and 80 % of RH, to 14.781 ± 2.501 and then to 15.369
363 ± 1.829 ‰ at 60 and 40 % RH, respectively (fig. 1b; Table 1). For 100 % RH, the high standard
364 deviations (SD) associated with $\delta^{18}O_{LW}$ (table S1), and consequently with $\Delta^{18}_{LW\text{-}IW}$ (Table 1), are
365 due to the very high $\delta^{18}O_{LW}$ value of sample P3-100-10-05-16. However, as we do not have any
366 explanation for this high value, this data was not withdrawn from the dataset. The ^{17}O-excess
367 values associated with the enrichment $\Delta^{18}_{LW\text{-}IW}$ (or $^{17}O\text{-excess}_{e\ LW\text{-}IW} = \ln(\Delta^{17}O_{LW\text{-}IW} + 1) - 0.528$
368 x $\ln(\Delta^{18}O_{LW\text{-}IW} + 1)$) are scattered for a given RH. The averaged value however follows a clear
369 pattern (fig. 1c; table 1): it is relatively similar at 100 and 80 % RH (-88 ± 48 and -75 ± 20 per
370 meg, respectively) and decreases to -132 ± 41 and then to -159 ± 9 per meg, at 60 and 40 % of RH,
371 respectively. The relationship between $^{17}O\text{-excess}_{e\ LW\text{-}IW}$ and RH from 40 to 80 % (fig.1c) can be
372 expressed as follows:

373 $$^{17}O\text{-excess}_{e\ LW\text{-}IW} = 2.3 \times RH - 258 \qquad \text{Eq. 1}$$

374 where $^{17}O\text{-excess}_{e\ LW\text{-}IW}$ is expressed in per meg *vs* VSMOW and RH in %. R^2 is 0.72 and $p <$
375 0.0001 for the 95 % confidence interval. $\theta_{LW\text{-}IW}$ was calculated using the ln expression of $\Delta^{17}_{LW\text{-}IW}$ and $\Delta^{18}_{LW\text{-}IW}$. The raw values of $\theta_{LW\text{-}IW}$ do not show any significant trend with RH and average
377 0.519 ± 0.002 (table 1).

378 The average phytolith content ranges from 1.1 to 0.1% d.w. Silicification of the leaf blade of *F.*
379 *arundinacea* increases with increasing transpiration and decreasing humidity (Table 1). Phytolith
380 morphological identification shows that they formed preferentially in the epidermal short cell and
381 to a smaller extent in the epidermal long cells (fig. 2). The proportion of silicified long cells,
382 increases with increasing transpiration and decreasing RH (Table 1). Some hair and bulliform cells
383 were also silicified, but in much smaller quantities. $\delta'^{18}O$ and ^{17}O-excess of phytoliths ($\delta'^{18}O_{Phyto}$

Biogeosciences Discuss., https://doi.org/10.5194/bg-2017-471
Manuscript under review for journal Biogeosciences
Discussion started: 8 November 2017
© Author(s) 2017. CC BY 4.0 License.

and ^{17}O-excess$_{Phyto}$ respectively) show the same general trends with RH as $\delta'^{18}O_{LW}$ and ^{17}O-excess$_{LW}$ (fig. 1a, table S1).

The average value of the ^{18}O-enrichment of phytoliths relative to the bulk leaf water ($\Delta^{18}_{Phyto\text{-}LW}$) increases when RH decreases from 27.948 ± 7.168 and 28.422 ± 0.402‰ at 100 and 80 % of RH respectively to 29.335 ± 002.0 ‰ at 60 % of RH and then 32.259 ± 2.192 ‰ at 40% of RH (fig. 1b, Table 1). With regard to the enrichment of phytoliths relative to the irrigation water, $\Delta^{18}O_{Phyto\text{-}IW}$ shows the same feature as $\Delta^{18}O_{LW\text{-}IW}$, stabilizing from 100 to 80 % RH (36.167 ± 0.701 and 36.464 ± 0.461 ‰, respectively) and increasing from 80 to 40 %, to reach 48.695 ± 2.280‰ at 40 % RH (fig.1b, table 1). ^{17}O-excess$_{e\ Phyto\text{-}IW}$ decreases with RH (from -210 ± 3 to -381 ± 19 per meg from 100 to 40 % RH) (fig. 1c, Table 1) according to the following equation (Eq.2):

$$^{17}\text{O-excess}_{e\ Phyto\text{-}IW} = 4.4 \times RH - 554 \qquad \text{Eq. 2}$$

where ^{17}O-excess$_{e\ Phyto\text{-}IW}$ is expressed in per meg *vs* VSMOW and RH in %. R^2 is 0.94 and $p < 0.0001$ for the 95% confidence interval. This link between ^{17}O-excess$_{e\ Phyto\text{-}IW}$ and RH is mainly due to the leaf water ^{17}O-excess dependency to RH since no particular trend is observed between ^{17}Oexcess$_{e\ Phyto\text{-}LW}$ and RH and the raw values of $\theta_{Phyto\text{-}LW}$ appears constant, averaging 0.526 ± 0.004 (table 1). The coefficient, equivalent to 4.4 per meg / %, appears higher than the coefficient obtained for ^{17}O-excess$_{e\ LW\text{-}IW}$ *vs* RH (2.3 per meg / %). However, a Student's t-test (relevant when the variance of two data sets are equal; Andrade and Estévez-Pérez, 2014), calculated on the two data sets shows that for a 90% confidence interval, the slopes of the lines are not statistically different.

3.2 Natural samples

Values of $\delta^{18}O_{Phyto}$ and ^{17}O-excess$_{Phyto}$ range respectively from 24.075 to 38.901 ‰ and from -140 to -290 per meg (table 2). The variations are in the same order of magnitude as for the growth chamber experiment. The estimates of $\delta^{18}O_{Pre}$ vary little along the sampled transect (from -4.458 to –3.220 ‰). No relationship is observed between $\delta^{18}O_{phyto}$ or the ^{18}O-enrichment of phytoliths relatively to precipitation ($\Delta^{18}_{Phyto\text{-}Pre}$) and MAP, MAT or RH (fig. 3, table 2).

Although scattered, the ^{17}O-excess$_{Phyto}$ values show a significant correlation with RH (fig. 4), regardless of which RH variable is taken into account. After excluding two outliers, the slopes of the correlation lines are 2.1 and 2.2 when RH and RH15 are taken into account, 3.4 when either RH-rd0>1 or RH15-rd0>1 are considered. The relationship obtained between ^{17}O-excess$_{Phyto}$ and RH-rd0>1 is the closest to the one obtained between ^{17}O-excess$_{phyto}$ and RH in the growth chambers (fig. 4b). It can be expressed as follows (Eq.3):

$$^{17}\text{O-excess}_{phyto} = 3.4 \times (RH\text{-}rd0>1) - 460 \qquad (r^2 = 0.48;\ p < 0.001) \qquad \text{Eq. 3}$$

where ^{17}O-excess$_{phyto}$ is expressed in per meg *vs* VSMOW and RH in %.

The excluded outliers (Table 3) are RIM1 and C3L4. RIM1 presents a very low ^{17}O-excess (-305 per meg) relatively to the ^{17}O-excess of the samples with close RH-rd0>1, i.e. from 71 to 74 % (average of -237 ± 32 per meg for 82-78, 83-116 and 83-115). C3L4 is located next to C4L3 and

Biogeosciences Discuss., https://doi.org/10.5194/bg-2017-471
Manuscript under review for journal Biogeosciences
Discussion started: 8 November 2017
© Author(s) 2017. CC BY 4.0 License.

under similar averaged RH but presents a ^{17}O-excess higher by 133 per meg. RIM1 and C3L4 show morphological patterns very similar to the other assemblages with the same range of RH. Thus, the discrepancies may lie either in the fact that local RH variations may not be reflected in RH averaged estimates for 10' (≈ 185 km^2) or in the particularity of the isotope composition of the local soil water (see discussion below).

The phytolith index d/p ranges from 0.01 to 0.08 in savanna, from 0.14 to 0.49 in wooded savanna, from 0.76 to 1.58 in enclosed savanna and from 1.84 to 6.78 in humid forests (Table 2). This unambiguous increase of d/p with tree cover density is in agreement with previous calibrations performed for the West African area (Bremond et al., 2005b). Interestingly, under high RH conditions, humid forest and enclosed savanna that are characterized by a large range of d/p represent a small range of ^{17}O-excess. Conversely, under lower RH conditions, savanna and wooded savanna that are characterized by a small range of d/p represent a large range of ^{17}O-excess (fig.5). This absence of relationship between ^{17}O-excess and tree cover density is also mirrored in figure 4 where phytolith samples from different vegetation types (i.e. savanna *vs* wooded savanna or humid forests *vs* enclosed savanna), that have developed under the same RH conditions, have the same range of ^{17}O-excess.

4 Discussion

4.1 Imprint of changes in atmospheric RH on the ^{17}O-excess of leaf water

In the bulk leaf water, the trends observed between $\Delta^{18}_{LW\text{-}IW}$ or ^{17}O-excess$_{e\ LW\text{-}IW}$ and RH from 80 to 40 % are in agreement with an evaporative kinetic fractionation that increases when RH decreases, as expected from previous studies on the $^{18}\delta O_{LW}$ or ^{17}O-excess$_{LW}$ evolution (e.g. Cernusak et al., 2016; Landais et al., 2006; Li et al., 2017). The obtained averaged value of $\theta_{LW\text{-}IW}$ (0.519 ± 0.002) is close to the value of θ_{diff} calculated for the diffusion of vapor in air (0.518; Barkan and Luz, 2007). As schematically described in Landais et al. (2016), λ_{transp} (equivalent to $\theta_{LW\text{-}IW}$) represents the interplay among three processes in the leaf boundary layer: 1) the equilibrium fractionation, which is only temperature-dependent (Majoube, 1971) and drives the isotope composition of leaf water along the equilibrium water line (θ_{equil} = 0.529); 2) the diffusion transport leading to increasing kinetic fractionation with decreasing relative humidity along the diffusion line (θ_{diff} = 0.518); 3) the isotope exchange of leaf water with atmospheric water vapor, decreasing from turbulent to laminar and molecular leaf boundary layer vapor transport conditions (e.g. Buhay et al., 1996). In the case of the growth chamber experiment, the fact that $\theta_{LW\text{-}IW}$ is close to θ_{diff} supports that the increasing diffusion of vapor in air when RH decreases or transpiration increases is the main process controling the evolution of ^{17}O-excess$_{LW}$. At high humidity (80-100% RH), the kinetic fractionation likely reaches its minimum as the diffusion process becomes limited.

The $\delta^{18}O_{LW}$ is commonly modelled as a function of the isotope composition of absorbed water, the isotope composition of water vapor, and RH (Craig and Gordon, 1965). The Craig and Gordon simple approach overestimates $\delta^{18}O_{LW}$ and different corrections have been proposed to take into account the diffusion of the evaporating water back to the leaf lamina and the advection of less

© Author(s) 2017. CC BY 4.0 License.

459 evaporating stem water (i.e. the Péclet effect, Buhay et al., 1996; Helliker and Ehleringer, 2000;
460 Roden et al., 2000; Farquhar and Gan, 2003; Farquhar and Cernusak, 2005; Ripullone et al., 2008;
461 Treydte et al., 2014). In the growth chamber experiment, where water availability, relative
462 humidity, and temperature were kept constant, we assume that transpiration rapidly reached a
463 steady state and that the isotope composition of transpired water was the same as that of the
464 irrigation water entering the plant (e.g. Welp et al., 2008). A tentative estimate of the theoretical
465 value of $\Delta^{18}_{LW\text{-}IW}$, $\Delta^{17}_{LW\text{-}IW}$ and $^{17}O\text{-excess}_{e\ LW\text{-}IW}$ was performed using the equations proposed for
466 ^{18}O-enrichment by Cernusak et al. (2016) (table S2). For calculating the $\Delta^{17}_{LW\text{-}IW}$ we used for the
467 equilibrium and kinetic fractionations (respectively $^{17}\alpha_{eq}$ and $^{17}\alpha_{k}$ in table S2) $^{17}\alpha_{eq} = {}^{18}\alpha_{eq}{}^{0.529}$ and
468 $^{17}\alpha_{k} = {}^{18}\alpha_{eq}{}^{0.518}$. As expected, the predicted $\Delta^{18}_{LW\text{-}IW}$ values were all higher than the observed values
469 by several ‰, the differences showing an increase with decreasing RH. Helliker and Ehleringer
470 (2000) proposed, for monocotyledonous species characterized by a vertical parallel veinal
471 structure, to use instead of the Craig and Gordon model the Gat and Bowser (1991) equation
472 describing the movement of water through a sequence of pools in series. However this model
473 would further increase the estimates of $\Delta^{18}_{LW\text{-}IW}$. The predicted $^{17}O\text{-excess}_{e}$ was either higher or
474 lower than the observed $^{17}O\text{-excess}_{e\ LW\text{-}IW}$ by 4 to 64 per meg (and even by 131 per meg for the
475 outlier P3-100-10-05-16). Predicted $\theta_{LW\text{-}IW}$ increased with RH from 0.522 to 0.529 which is far
476 from the observed values averaging 0.519. The predicted value of 0.529 at 100 % RH reflects pure
477 equilibrium in a situation where irrigation water and water vapor are assumed to have similar
478 isotope composition since irrigation water is directly vaporized into the chamber (table S2),
479 without any fractionation. Sensitivity tests show that regardless of the model chosen (Buhay et al.,
480 1996; Cernusak et al., 2016; Li et al., 2017), estimations of $\theta_{LW\text{-}IW}$ are very dependant on the isotope
481 compositions of the water vapor (Li et al., 2017), not measured either in our experiment or in
482 previous studies (Landais et al., 2006; Li et al., 2017). In the natural environment, a first order
483 approximation for the isotope composition of water vapor is to consider equilibrium with
484 precipitation. A a result of water-vapor equilibrium fractionation and soil water ^{18}O-enrichment,
485 this can lead to a water vapor ^{18}O-depleted by 10-13 ‰ compared to the soil water (Landais et al.,
486 2006). In this case the predicted λ_{transp} (equivalent to $\theta_{LW\text{-}SW}$) decreases with increasing humidity.
487 Finally, because wrong values of the isotope compositions of the water vapor may affect
488 significantly the calculation of $\Delta^{18}_{LW\text{-}IW}$, $\Delta^{17}O\text{-excess}_{e\ LW\text{-}IW}$ and $\theta_{LW\text{-}SW}$, we call for vapor isotope
489 measurements as a prerequisite to accurately model the leaf water triple oxygen isotope evolution
490 with RH. However, overall, despite the uncertainties on the predicted evolution of $\theta_{LW\text{-}SW}$ with RH,
491 the predicted value of $^{17}O\text{-excess}_{e\ LW\text{-}IW}$ decreases when RH increases, which is also observed, as
492 well as reflected in the triple isotope composition of phytoliths, as discussed below.

493 4.2 Imprint of changes in atmospheric RH on the ^{17}O-excess of phytoliths

494 Polymerization of silica is supposed to occur in isotope equilibrium with the forming-water, and
495 therefore, to be only governed by temperature and the isotope composition of the forming water.
496 Almost a dozen temperature-dependant relationships have been empirically established between
497 the $\delta^{18}O$ of quartz, sinters, cherts, diatoms or phytoliths and the $\delta^{18}O$ of their forming water

Biogeosciences Discuss., https://doi.org/10.5194/bg-2017-471
Manuscript under review for journal Biogeosciences
Discussion started: 8 November 2017
© Author(s) 2017. CC BY 4.0 License.

498 ($\delta^{18}_{PhytoFW}$). Although the obtained fractionation coefficients are close (from -0.2 to -0.4 ‰ $°C^{-1}$),
499 the range of fractionation ($\Delta^{18}_{Phyto\text{-}PhytoFW}$) is large (see synthesis in Alexandre et al., 2012). The
500 $\Delta^{18}_{Phyto\text{-}LW}$ values obtained in the frame of the growth chamber experiment (ranging from 27.9 ±
501 7.2 to 32.3 ± 2.2‰) encompass the $\Delta^{18}_{Phyto\text{-}PhytoFW}$ of 31.1‰ calculated from the Dodd and Sharp
502 (2010) relationship for 25°C. It is lower than the values of 36.4 and 36 ‰ at 25 °C, calculated from
503 Sharp et al. (2016) and Alexandre et al. (2012). Whereas Alexandre et al. (2012) and Sharp et al.
504 (2016) generally estimated the forming-water $\delta^{18}O$ values, Dodd and Sharp (2010) measured the
505 the $\delta^{18}O$ values of the water samples. The proximity of the obtained range of $\Delta^{18}_{Phyto\text{-}LW}$ values to
506 the $\Delta^{18}_{Phyto\text{-}Phyto\ FW}$ calculated from Dodd and Sharp (2010) suggests that phytoliths formed in
507 equilibrium with a water of isotope composition close to that of the bulk leaf water. This is
508 additionally supported by the obtained averaged value of $\theta_{Phyto\text{-}LW}$ (0.526 ± 0.004), which is close
509 to the $\theta_{SiO2\text{-}water}$ equilibrium value of 0.524 calculated for 25 °C from Sharp et al. (2016).

510 Evolution of the triple isotope composition of bulk leaf water and phytoliths can be illustrated by
511 plotting $\delta'^{17}O$ *vs* $\delta'^{18}O$, or ^{17}O-excess *vs* $\delta'^{18}O$ (fig. 6) which is more appropriate to evidence small
512 variations. Figure 6 shows that the leaf water evolved from the irrigation water pool, becomes
513 increasingly subject to kinetic fractionation when RH decreased. This evolution follows a single
514 leaf water line reflecting $\theta_{LW\text{-}IW}$ = 0.519 (Table1). Then, if phytoliths polymerized from the bulk
515 leaf waters, at 25°C, according to a constant equilibrium fractionation ($\Delta^{18}_{Phyto\text{-}LW}$ value close to
516 31.1‰; $\theta_{Phyto\text{-}IW}$ close to 0.524-0.526), the expected phytolith line in the ^{17}O-excess *vs* $\delta'^{18}O$
517 diagram should be parallel to the leaf water line. Although the slope of the observed phytolith line
518 appears slightly different from the expected one, a Student's t-test calculated on the leaf water and
519 phytolith data sets shows that for a 90 % confidence interval, the slopes are not statistically
520 different. This would support that phytoliths basically polymerized from the bulk leaf water and
521 that evolution of their triple isotope composition is governed by that of the bulk leaf water, itself
522 controlled by RH. However, when looking closer at the difference between $\delta'^{18}O_{Phyto}$ and $\delta'^{18}O_{LW}$
523 (fig. 6) or at $\Delta^{18}O_{Phyto\text{-}LW}$ (Table 1), for a given *F. arundinacea* sample, a significant increase can
524 be observed when RH reaches 40 %. This indicates, on the contrary, a phytolith-forming water
525 different from the bulk leaf water and more subject to kinetic fractionation. The Péclet effect,
526 which is known to scale with transpiration (e.g. Barnard et al., 2007) can explain this discrepancy.
527 Advection of less evaporated stem water may decrease $\delta^{18}O_{LW}$ and increase $^{17}O\text{-excess}_{LW}$
528 relatively to $\delta^{18}O$ and ^{17}O-excess of the epidermal water prone to evaporation and from which
529 phytoliths formed. This is however not shown by the $^{17}O\text{-excess}_{e\ Phyto\text{-}LW}$ values, that are not
530 significantly lower than that obtained at higher RH (except for one sample). At this point, the data
531 scattering prevents further discussion but the discrepancy between $\Delta^{18}O_{Phyto\text{-}LW}$ and $^{17}O\text{-excess}_{e}$
532 $_{Phyto\text{-}LW}$ evolutions at low RH and the possibility that the phytolith forming-water is different from
533 the bulk leaf water must be investigated in future research developments.

534 With regard to the natural samples, whereas no relationship was found between $\delta^{18}O_{phyto}$ and RH,
535 a clear dependency of $^{17}O\text{-excess}_{phyto}$ to RH was shown, equivalent to 2.1 per meg / % when the

Biogeosciences Discuss., https://doi.org/10.5194/bg-2017-471
Manuscript under review for journal Biogeosciences
Discussion started: 8 November 2017
© Author(s) 2017. CC BY 4.0 License.

536 annual RH average was taken into account, or to 3.4 per meg / % when the average of the growing
537 season (RH-rd0>1) was taken into account (fig. 4). These coefficients are in the range of those
538 obtained for the growth chamber experiment for $^{17}O\text{-excess}_{Phyto}$, $^{17}O\text{-excess}_{e\ LW\text{-}IW}$ and $^{17}O\text{-excess}_{e}$
539 $_{Phyto\text{-}IW}$. This consistency represents a major positive step in examining whether changes in
540 atmospheric RH imprint the ^{17}O-excess of natural phytolith assemblages in a predictable way. The
541 data scattering (r^2 = 0.48 to 0.51, $p < 0.001$) however call for taking into account additional
542 parameters beside RH that can contribute to changes in $^{17}O\text{-excess}_{Phyto}$. One can expect the isotope
543 composition of the soil water taken-up by the roots to impact $^{17}O\text{-excess}_{Phyto}$. In tropical dry and
544 humid areas, evaporative kinetic fractionation can lead to a ^{18}O-enrichment of the soil water of
545 several ‰, in the first dm depth (e.g. Gaj et al., 2016; Liu et al., 2010). Spatial variability in the
546 composition of the rainfall feeding the upper soil water may also intervene. However, the amount-
547 weighted values of $\delta^{18}O_{Pre}$ along the sampled transect vary little (Table 2). With regard to ^{17}O-
548 excess, changes in soil water evaporation rather than the small variations expected for ^{17}O-
549 $excess_{Pre}$ (Landais et al., 2010b; Li et al., 2015) should impact the evolution of $^{17}O\text{-excess}_{Phyto}$,
550 although, here, the lack of measurements only allow for speculation.

551 The source vegetation of the phytolith assemblages may also bring some noise to the relationship
552 between $^{17}O\text{-excess}_{phyto}$ and RH. The Globular granulate phytoliths that are assumed to come from
553 the non-transpiring secondary xylem of the wood should present an isotope signature closer to that
554 of the soil water, or less impacted by kinetic fractionation than the grass phytoliths. However, for
555 a given range of RH, samples with significant representations of both phytolith categories (i.e
556 wooded savanna and enclosed savanna with d/p from 0.1 to 1.6) present ^{17}O-excess values close
557 to the values obtained by samples with very low or very high d/p (figs. 4 and 5). To further assess
558 the significance of the Globular granulate isotope signature, we calculated $\delta^{18}O_{PhytoFW}$ values
559 (Table 2) using the Dodd and Sharp (2010) fractionation factor and compared it to the
560 precipitation-weighted $\delta^{18}O_{Pre\text{-}rd0>1}$ average. For the humid forest assemblages, $\delta^{18}O_{PhytoFW}$ values
561 are higher than $\delta^{18}O_{pre\ rd0>1}$ by 5 ± 1.4 ‰. This difference is larger than the range of ^{18}O-enrichment
562 observed for the tenths upper cm depth of soil water under tropical humid forests (2-3‰; Liu et
563 al., 2008; Stahl et al., 2013), suggesting that evaporative isotope signatures of both soils and leaf
564 water imprinted the Globular granulate phytolith type. Complementary examination of the isotope
565 signature of phytolith assemblages from forests growing under different RH conditions (i.e dry
566 forests, humid forests, rainforests), as well as further investigation of the anatomical origin of the
567 Globular granulate phytolith type are now required to further discuss the meaning of the ^{17}O-excess
568 signal brought by tropical forest phytolith assemblages.

569 Biases due to the calibration methodology may also be responsible for the data scattering.
570 Imperfect adequation between the space scales recorded by the soil top phytolith assemblages and
571 the RH variables may come into play. Phytolith assemblages represent a mixture of local and wind-
572 transported phytoliths. In the open saharian, sahelian and soudanian zones of West Africa the
573 winter low altitude north-easterly trade winds may transport phytoliths southward, reducing
574 differences between assemblages from different biogeographic zones and increasing differences
575 among assemblages of a given biogeographic zone (Bremond et al., 2005b). Additional samples

© Author(s) 2017. CC BY 4.0 License.

576 from other geographic zones are thus needed to increase the robustness of the relationship. With
577 regard to the recorded time scales, phytolith assemblages likely record several decades of phytolith
578 production in agreement with the CRU RH 30 years averages.

579 **5 Conclusion**

580 The present combination of growth chamber and i*n situ* transect calibrations lay the groundwork
581 for further examination of the robustness of the $^{17}O\text{-excess}_{Phyto}$ as a proxy of changes in RH. The
582 growth chamber experiment demonstrated that change in RH imprint the $^{17}O\text{-excess}_{e\ Phyto\text{-}IW}$ (by
583 4.4 per meg / %) through its imprint on $^{17}O\text{-excess}_{e\ LW\text{-}IW}$. As the isotope composition of the
584 irrigation water was stable, and transpiration likely reached a steady state, the positive correlation
585 between $^{17}O\text{-excess}_{LW}$ and RH was only governed by the kinetic fractionation occurring in the leaf
586 epidermis water subject to evaporation, as supported by the value of $\theta_{LW\text{-}IW}$ of 0.519, close to θ_{diff}.

587 In order to model the triple oxygen isotope fractionation in play at the soil/plant/atmosphere
588 interface we require direct and continuous measurements of the triple isotope composition of water
589 vapor. Such measurements should develop in the near futur through the use of isotope ratio infrared
590 analyzers (e.g. Berkelhammer et al., 2013; Schmidt et al., 2010). We also suggest to constrain as
591 much as possible the isotope composition of the soil water taken up by the roots. Stem water is
592 usually used as an analogue of soil water when modelling $\delta'^{17}O_{LW}$ and $\delta'^{18}O_{LW}$ (Landais et al.,
593 2006; Li et al., 2017). However, in the stem, water in the phloem that is bidirectional (moves up
594 and down the plant's stem) receives the contribution of evaporating leaf water, whereas water in
595 the xylem that is unidirectional (moves up the plant's stem) is not influenced by leaf evaporation.
596 Consequently one may expect the isotope composition of stem water to be slightly different than
597 that of soil water (Berkelhammer et al., 2013; Treydte et al., 2014).

598 When plotting $^{17}O\text{-excess}_{Phyto}$ *vs* RH, the samples collected along the West and Central African
599 relative humidity transect lay close to the growth chamber $^{17}O\text{-excess}_{e\ phyto\text{-}IW}$ line and define a
600 correlation coefficient ranging from 2.1 to 3.4 per meg / % (depending on the RH variable taken
601 into account). This supports that RH is an important control of $^{17}O\text{-excess}_{Phyto}$ in natural
602 environment, even if phytolith assemblages come from different vegetation types. However, other
603 parameters such as changes in the triple isotope composition of the soil water or imperfect
604 adequation between the space scales recorded by the soil top phytolith assemblages and the RH
605 variables may come into play and explain the scattering of $^{17}O\text{-excess}_{Phyto}$. Assessment of these
606 parameters through additional growth chambers experiments and field campaigns will bring us
607 closer to an accurate proxy of changes in relative humidity.

608

609 *Acknowledgements*

610 This study was supported by the French program INSU-LEFE and benefited from the CNRS
611 human and technical resources allocated to the ECOTRONS Research Infrastructures as well as
612 from the state allocation 'Investissements d'Avenir' ANR-11-INBS-0001.

613

© Author(s) 2017. CC BY 4.0 License.

References

Affolter, S., Häuselmann, A.D., Fleitmann, D., Häuselmann, P., and Leuenberger, M. (2015). Triple isotope (δD, δ17O, δ18O) study on precipitation, drip water and speleothem fluid inclusions for a Western Central European cave (NW Switzerland). Quat. Sci. Rev. *127*, 73–89.

Alexandre, A., and Brémond, L. (2009). Comment on the paper in Quaternary International: "Methodological concerns for analysis of phytolith assemblages: Does count size matter?" (C.A.E. Strömberg). Quat. Int. *193*, 141–142.

Alexandre, A., Meunier, J.-D., Colin, F., and Koud, J.-M. (1997). Plant impact on the biogeochemical cycle of silicon and related weathering processes. Geochim. Cosmochim. Acta *61*, 677–682.

Alexandre, A., Crespin, J., Sylvestre, F., Sonzogni, C., and Hilbert, D.W. (2012). The oxygen isotopic composition of phytolith assemblages from tropical rainforest soil tops (Queensland, Australia): validation of a new paleoenvironmental tool. Clim. Past *8*, 307–324.

Alexandre, A., Balesdent, J., Cazevieille, P., Chevassus-Rosset, C., Signoret, P., Mazur, J.-C., Harutyunyan, A., Doelsch, E., Basile-Doelsch, I., Miche, H., et al. (2016). Direct uptake of organically derived carbon by grass roots and allocation in leaves and phytoliths: 13C labeling evidence. Biogeosciences *13*, 1693–1703.

Alexandre, A.E., Pailles, C., Sonzogni, C., Kershaw, P., Wust, R.A., and Turney, C.S. (2013). d18O signature of phytoliths from the last interglacial Lynch's Crater sediments (Qld, Australia): insights on changes in precipitation sources. AGU Fall Meet. Abstr. *33*.

Andrade, J.M., and Estévez-Pérez, M.G. (2014). Statistical comparison of the slopes of two regression lines: A tutorial. Anal. Chim. Acta *838*, 1–12.

Angert, A., Rachmilevitch, S., Barkan, E., and Luz, B. (2003). Effects of photorespiration, the cytochrome pathway, and the alternative pathway on the triple isotopic composition of atmospheric O2. Glob. Biogeochem. Cycles *17*, 1030.

Angert, A., Cappa, C.D., and DePaolo, D.J. (2004). Kinetic O-17 effects in the hydrologic cycle: Indirect evidence and implications. Geochim. Cosmochim. Acta *68*, 3487–3495.

Backwell, L.R., McCarthy, T.S., Wadley, L., Henderson, Z., Steininger, C.M., Bonita deKlerk, Barré, M., Lamothe, M., Chase, B.M., Woodborne, S., et al. (2014). Multiproxy record of late Quaternary climate change and Middle Stone Age human occupation at Wonderkrater, South Africa. Quat. Sci. Rev. *99*, 42–59.

Barkan, E., and Luz, B. (2005). High precision measurements of 17O/16O and 18O/16O ratios in H2O. Rapid Commun. Mass Spectrom. *19*, 3737–3742.

Barkan, E., and Luz, B. (2007). Diffusivity fractionations of H2(16)O/H2(17)O and H2(16)O/H2(18)O in air and their implications for isotope hydrology. Rapid Commun. Mass Spectrom. RCM *21*, 2999–3005.

Barnard, R.L., Salmon, Y., Kodama, N., Sörgel, K., Holst, J., Rennenberg, H., Gessler, A., and Buchmann, N. (2007). Evaporative enrichment and time lags between delta18O of leaf water and organic pools in a pine stand. Plant Cell Environ. *30*, 539–550.

Bartlein, P.J., Harrison, S.P., Brewer, S., Connor, S., Davis, B. a. S., Gajewski, K., Guiot, J., Harrison-Prentice, T.I., Henderson, A., Peyron, O., et al. (2010). Pollen-based continental climate reconstructions at 6 and 21 ka: a global synthesis. Clim. Dyn. *37*, 775–802.

Berkelhammer, M., Hu, J., Bailey, A., Noone, D.C., Still, C.J., Barnard, H., Gochis, D., Hsiao, G.S., Rahn, T., and Turnipseed, A. (2013). The nocturnal water cycle in an open-canopy forest. J. Geophys. Res. Atmospheres *118*, 10,225-10,242.

Bony, S., Colman, R., Kattsov, V.M., Allan, R.P., Bretherton, C.S., Dufresne, J.L., Hall, A.,

© Author(s) 2017. CC BY 4.0 License.

660 Hallegatte, S., Holland, M.M., Ingram, W., et al. (2006). How well do we understand and
661 evaluate climate change feedback processes? J. Clim. *19*, 3445–3482.
662 Bowen, G.J., and Revenaugh, J. (2003). Interpolating the isotopic composition of modern
663 meteoric precipitation. Water Resour. Res. *39*, 1299.
664 Bowen, G.J., and Wilkinson, B. (2002). Spatial distribution of δ18O in meteoric precipitation.
665 Geology *30*, 315–318.
666 Bowen, G.J., Wassenaar, L.I., and Hobson, K.A. (2005). Global application of stable hydrogen
667 and oxygen isotopes to wildlife forensics. Oecologia *143*, 337–348.
668 Bowling, D.R., Schulze, E.S., and Hall, S.J. (2017). Revisiting streamside trees that do not use
669 stream water: can the two water worlds hypothesis and snowpack isotopic effects explain a
670 missing water source? Ecohydrology *10*, n/a-n/a.
671 Bremond, L., Alexandre, A., Hely, C., and Guiot, J. (2005a). A phytolith index as a proxy of tree
672 cover density in tropical areas: Calibration with Leaf Area Index along a forest-savanna transect
673 in southeastern Cameroon. Glob. Planet. Change *45*, 277–293.
674 Bremond, L., Alexandre, A., Peyron, O., and Guiot, J. (2005b). Grass water stress estimated
675 from phytoliths in West Africa. J. Biogeogr. *32*, 311–327.
676 Bremond, L., Alexandre, A., Peyron, O., and Guiot, J. (2005c). Grass water stress estimated from
677 phytoliths in West Africa. J. Biogeogr. *32*, 311–327.
678 Buhay, W.M., Edwards, T.W.D., and Aravena, R. (1996). Evaluating kinetic fractionation
679 factors used for reconstructions from oxgen and hydrogen isotope ratios in plant water and
680 cellulose. Geochim. Cosmochim. Acta *60*, 2209–2218.
681 Cernusak, L.A., Barbour, M.M., Arndt, S.K., Cheesman, A.W., English, N.B., Feild, T.S.,
682 Helliker, B.R., Holloway-Phillips, M.M., Holtum, J.A.M., Kahmen, A., et al. (2016). Stable
683 isotopes in leaf water of terrestrial plants. Plant Cell Environ. *39*, 1087–1102.
684 Chapligin, B., Leng, M.J., Webb, E., Alexandre, A., Dodd, J.P., Ijiri, A., Lücke, A., Shemesh,
685 A., Abelmann, A., Herzschuh, U., et al. (2011). Inter-laboratory comparison of oxygen isotope
686 compositions from biogenic silica. Geochim. Cosmochim. Acta *75*, 7242–7256.
687 Chen, G., Auerswald, K., and Schnyder, H. (2016). 2H and 18O depletion of water close to
688 organic surfaces. Biogeosciences *13*, 3175–3186.
689 Chung, E.-S., Soden, B., Sohn, B.J., and Shi, L. (2014). Upper-tropospheric moistening in
690 response to anthropogenic warming. Proc. Natl. Acad. Sci. *111*, 11636–11641.
691 Collura, L.V., and Neumann, K. (2017). Wood and bark phytoliths of West African woody
692 plants. Quat. Int. *434*, *Part B*, 142–159.
693 Contreras, D.A., Robin, V., Gonda, R., Hodara, R., Dal Corso, M., and Makarewicz, C. (2014).
694 (Before and) After the Flood: A multiproxy approach to past floodplain usage in the middle
695 Wadi el-Hasa, Jordan. J. Arid Environ. *110*, 30–43.
696 Crespin, J., Alexandre, A., Sylvestre, F., Sonzogni, C., Paillès, C., and Garreta, V. (2008). IR
697 laser extraction technique applied to oxygen isotope analysis of small biogenic silica samples.
698 Anal. Chem. *80*, 2372–2378.
699 Delattre, H., Vallet-Coulomb, C., and Sonzogni, C. (2015). Deuterium excess in atmospheric
700 water vapor of a Mediterranean coastal wetland: regional versus local signatures. Atmos Chem
701 Phys Discuss *15*, 1703–1746.
702 Dessler, A.E., and Davis, S.M. (2010). Trends in tropospheric humidity from reanalysis systems.
703 J. Geophys. Res. Atmospheres *115*, D19127.
704 Dodd, J.P., and Sharp, Z.D. (2010). A laser fluorination method for oxygen isotope analysis of
705 biogenic silica and a new oxygen isotope calibration of modern diatoms in freshwater

© Author(s) 2017. CC BY 4.0 License.

environments. Geochim. Cosmochim. Acta *74*, 1381–1390.
Evaristo, J., Jasechko, S., and McDonnell, J.J. (2015). Global separation of plant transpiration from groundwater and streamflow. Nature *525*, 91–94.
Farquhar, G.D., and Cernusak, L.A. (2005). On the isotopic composition of leaf water in the non-steady state. Funct. Plant Biol. *32*, 293–303.
Farquhar, G.D., and Gan, K.S. (2003). On the progressive enrichment of the oxygen isotopic composition of water along a leaf. Plant Cell Environ. *26*, 801–819.
Fischer, E.M., and Knutti, R. (2013). Robust projections of combined humidity and temperature extremes. Nat. Clim. Change *3*, 126–130.
Gaj, M., Beyer, M., Koeniger, P., Wanke, H., Hamutoko, J., and Himmelsbach, T. (2016). In situ unsaturated zone water stable isotope (2 H and 18 O) measurements in semi-arid environments: a soil water balance. Hydrol. Earth Syst. Sci. *20*, 715–731.
Gat, J., and Bowser, C. (1991). Stable Isotope Geochemistry: A Tribute to Samuel Epstein (The Geochemical Society Special Publication No. 3).
Gázquez, F., Mather, I., Rolfe, J., Evans, N.P., Herwartz, D., Staubwasser, M., and Hodell, D.A. (2015). Simultaneous analysis of 17O/16O, 18O/16O and 2H/1H of gypsum hydration water by cavity ring-down laser spectroscopy. Rapid Commun. Mass Spectrom. *29*, 1997–2006.
Grießinger, J., Bräuning, A., Helle, G., Hochreuther, P., and Schleser, G. (2016). Late Holocene relative humidity history on the southeastern Tibetan plateau inferred from a tree-ring δ18O record: Recent decrease and conditions during the last 1500 years. Quat. Int.
Guillevic, M., Bazin, L., Landais, A., Stowasser, C., Masson-Delmotte, V., Blunier, T., Eynaud, F., Falourd, S., Michel, E., Minster, B., et al. (2014). Evidence for a three-phase sequence during Heinrich Stadial 4 using a multiproxy approach based on Greenland ice core records. Clim Past *10*, 2115–2133.
Held, I.M., and Soden, B.J. (2000). Water Vapor Feedback and Global Warming1. Annu. Rev. Energy Environ. *25*, 441–475.
Helliker, B.R., and Ehleringer, J.R. (2000). Establishing a grassland signature in veins: 18O in the leaf water of C3 and C4 grasses. Proc. Natl. Acad. Sci. U. S. A. *97*, 7894–7898.
Herbert, A.V., and Harrison, S.P. (2016). Evaluation of a modern-analogue methodology for reconstructing Australian palaeoclimate from pollen. Rev. Palaeobot. Palynol. *226*, 65–77.
Herwartz, D., Pack, A., Krylov, D., Xiao, Y., Muehlenbachs, K., Sengupta, S., and Rocco, T.D. Proceedings of the National Academy of Sciences.
IAEA (2013). A Laboratory Information Management System for Stable Hydrogen and Oxygen Isotopes in Water Samples by Laser Absorption Spectroscopy. User Manual & Tutorial.
Kool, D.M., Wrage, N., Oenema, O., Van Kessel, C., and Van Groenigen, J.W. (2011). Oxygen exchange with water alters the oxygen isotopic signature of nitrate in soil ecosystems. Soil Biol. Biochem. *43*, 1180–1185.
Kriticos, D.J., Webber, B.L., Leriche, A., Ota, N., Macadam, I., Bathols, J., and Scott, J.K. (2012). CliMond: global high-resolution historical and future scenario climate surfaces for bioclimatic modelling. Methods Ecol. Evol. *3*, 53–64.
Kumar, S., Milstein, Y., Brami, Y., Elbaum, M., and Elbaum, R. (2017). Mechanism of silica deposition in sorghum silica cells. New Phytol. *213*, 791–798.
Labuhn, I., Daux, V., Girardclos, O., Stievenard, M., Pierre, M., and Masson-Delmotte, V. (2015). French summer droughts since 1326 AD: a reconstruction based on tree ring cellulose δ18O. Clim Past Discuss *11*, 5113–5155.
Labuhn, I., Daux, V., Girardclos, O., Stievenard, M., Pierre, M., and Masson-Delmotte, V.

© Author(s) 2017. CC BY 4.0 License.

(2016). French summer droughts since 1326 CE: a reconstruction based on tree ring cellulose δ18O. Clim Past *12*, 1101–1117.
Landais, A., Barkan, E., Yakir, D., and Luz, B. (2006). The triple isotopic composition of oxygen in leaf water. Geochim. Cosmochim. Acta *70*, 4105–4115.
Landais, A., Barkan, E., and Luz, B. (2008). Record of δ18O and 17O-excess in ice from Vostok Antarctica during the last 150,000 years. Geophys. Res. Lett. *35*, L02709.
Landais, A., Dreyfus, G., Capron, E., Masson-Delmotte, V., Sanchez-Goñi, M.F., Desprat, S., Hoffmann, G., Jouzel, J., Leuenberger, M., and Johnsen, S. (2010a). What drives the millennial and orbital variations of δ18Oatm? Quat. Sci. Rev. *29*, 235–246.
Landais, A., Risi, C., Bony, S., Vimeux, F., Descroix, L., Falourd, S., and Bouygues, A. (2010b). Combined measurements of 17Oexcess and d-excess in African monsoon precipitation: Implications for evaluating convective parameterizations. Earth Planet. Sci. Lett. *298*, 104–112.
Lavergne, A., Daux, V., Villalba, R., Pierre, M., Stievenard, M., and Srur, A.M. (2017). Improvement of isotope-based climate reconstructions in Patagonia through a better understanding of climate influences on isotopic fractionation in tree rings. Earth Planet. Sci. Lett. *459*, 372–380.
Lezine, A.M. (1988). New pollen data from the Sahel, Senegal. In Review of Palaeobotany and Palynology, (Elsevier), pp. 141–154.
Li, S., Levin, N.E., and Chesson, L.A. (2015). Continental scale variation in 17O-excess of meteoric waters in the United States. Geochim. Cosmochim. Acta *164*, 110–126.
Li, S., Levin, N.E., Soderberg, K., Dennis, K.J., and Caylor, K.K. (2017). Triple oxygen isotope composition of leaf waters in Mpala, central Kenya. Earth Planet. Sci. Lett. *468*, 38–50.
Liu, W., Liu, W., Li, P., Duan, W., and Li, H. (2010). Dry season water uptake by two dominant canopy tree species in a tropical seasonal rainforest of Xishuangbanna, SW China. Agric. For. Meteorol. *150*, 380–388.
Liu, W.J., Liu, W.Y., Li, J.T., Wu, Z.W., and Li, H.M. (2008). Isotope variations of throughfall, stemflow and soil water in a tropical rain forest and a rubber plantation in Xishuangbanna, SW China. Hydrol. Res. *39*, 437–449.
Luz, B., and Barkan, E. (2010). Variations of 17O/16O and 18O/16O in meteoric waters. Geochim. Cosmochim. Acta *74*, 6276–6286.
Ma, J.F., and Yamaji, N. (2006). Silicon uptake and accumulation in higher plants. Trends Plant Sci. *11*, 392–397.
Ma, J.F., Tamai, K., Yamaji, N., Mitani, N., Konishi, S., Katsuhara, M., Ishiguro, M., Murata, Y., and Yano, M. (2006). A silicon transporter in rice. Nature *440*, 688–691.
Madella, M., Alexandré, A., Ball, T., Group, I.W., and others (2005). International code for phytolith nomenclature 1.0. Ann. Bot. *96*, 253–260.
Majoube, M. (1971). Fractionnement en oxygène 18 et en deutérium entre l'eau et sa vapeur. J. Chim. Phys. *68*, 1423–1436.
Martín-Gómez, P., Barbeta, A., Voltas, J., Peñuelas, J., Dennis, K., Palacio, S., Dawson, T.E., and Ferrio, J.P. (2015). Isotope-ratio infrared spectroscopy: a reliable tool for the investigation of plant-water sources? New Phytol. *207*, 914–927.
Miller, M.F. (2002). Isotopic fractionation and the quantification of 17O anomalies in the oxygen three-isotope system: an appraisal and geochemical significance. Geochim. Cosmochim. Acta *66*, 1881–1889.
Miller, M.F., Greenwood, R.C., and Franchi, I.A. (2015). Comment on "The triple oxygen isotope composition of the Earth mantle and understanding Δ17O variations in terrestrial rocks

© Author(s) 2017. CC BY 4.0 License.

and minerals" by Pack and Herwartz [Earth Planet. Sci. Lett. 390 (2014) 138–145]. ResearchGate *418*.
New, M., Lister, D., Hulme, M., and Makin, I. (2002). A high-resolution data set of surface climate over global land areas. Clim. Res. *21*, 1–25.
Oerter, E., Finstad, K., Schaefer, J., Goldsmith, G.R., Dawson, T., and Amundson, R. (2014). Oxygen isotope fractionation effects in soil water via interaction with cations (Mg, Ca, K, Na) adsorbed to phyllosilicate clay minerals. J. Hydrol. *515*, 1–9.
Orlowski, N., Pratt, D.L., and McDonnell, J.J. (2016). Intercomparison of soil pore water extraction methods for stable isotope analysis. Hydrol. Process. *30*, 3434–3449.
Pack, A., and Herwartz, D. (2014). The triple oxygen isotope composition of the Earth mantle and understanding variations in terrestrial rocks and minerals. Earth Planet. Sci. Lett. *390*, 138–145.
Passey, B.H., Hu, H., Ji, H., Montanari, S., Li, S., Henkes, G.A., and Levin, N.E. (2014). Triple oxygen isotopes in biogenic and sedimentary carbonates. Geochim. Cosmochim. Acta *141*, 1–25.
Piperno, D.R. (2006). Phytoliths: A Comprehensive Guide for Archaeologists and Paleoecologists (Rowman Altamira).
Ripullone, F., Matsuo, N., Stuart-Williams, H., Wong, S.C., Borghetti, M., Tani, M., and Farquhar, G. (2008). Environmental Effects on Oxygen Isotope Enrichment of Leaf Water in Cotton Leaves. Plant Physiol. *146*, 729–736.
Risi, C., Landais, A., Bony, S., Jouzel, J., Masson-Delmotte, V., and Vimeux, F. (2010). Understanding the 17O excess glacial-interglacial variations in Vostok precipitation. J. Geophys. Res. Atmospheres *115*, D10112.
Risi, C., Landais, A., Winkler, R., and Vimeux, F. (2013). Can we determine what controls the spatio-temporal distribution of d-excess and 17O-excess in precipitation using the LMDZ general circulation model? Clim Past *9*, 2173–2193.
Schmidt, M., Maseyk, K., Lett, C., Biron, P., Richard, P., Bariac, T., and Seibt, U. (2010). Concentration effects on laser-based δ18O and δ2H measurements and implications for the calibration of vapour measurements with liquid standards. Rapid Commun. Mass Spectrom. *24*, 3553–3561.
Schwab, V.F., Garcin, Y., Sachse, D., Todou, G., Séné, O., Onana, J.-M., Achoundong, G., and Gleixner, G. (2015). Effect of aridity on δ13C and δD values of C3 plant- and C4 graminoid-derived leaf wax lipids from soils along an environmental gradient in Cameroon (Western Central Africa). Org. Geochem. *78*, 99–109.
Scurfield, G., Anderson, and Segnit (1974). Silica in woody stems. Aust. J. Bot *22*, 211–229.
Sharp, Z.D., Gibbons, J.A., Maltsev, O., Atudorei, V., Pack, A., Sengupta, S., Shock, E.L., and Knauth, L.P. (2016). A calibration of the triple oxygen isotope fractionation in the SiO2–H2O system and applications to natural samples. Geochim. Cosmochim. Acta *186*, 105–119.
Sherwood, S.C., Ingram, W., Tsushima, Y., Satoh, M., Roberts, M., Vidale, P.L., and O'Gorman, P.A. (2010). Relative humidity changes in a warmer climate. J. Geophys. Res. Atmospheres *115*, D09104.
Stahl, C., Hérault, B., Rossi, V., Burban, B., Bréchet, C., and Bonal, D. (2013). Depth of soil water uptake by tropical rainforest trees during dry periods: does tree dimension matter? Oecologia *173*, 1191–1201.
Steig, E.J., Gkinis, V., Schauer, A.J., Schoenemann, S.W., Samek, K., Hoffnagle, J., Dennis, K.J., and Tan, S.M. (2014). Calibrated high-precision 17O-excess measurements using cavity ring-down spectroscopy with laser-current-tuned cavity resonance. Atmospheric Meas. Tech. *7*,

© Author(s) 2017. CC BY 4.0 License.

2421–2435.
Treydte, K., Boda, S., Graf Pannatier, E., Fonti, P., Frank, D., Ullrich, B., Saurer, M., Siegwolf, R., Battipaglia, G., Werner, W., et al. (2014). Seasonal transfer of oxygen isotopes from precipitation and soil to the tree ring: source water versus needle water enrichment. New Phytol. *202*, 772–783.
Tuthorn, M., Zech, R., Ruppenthal, M., Oelmann, Y., Kahmen, A., del Valle, H.F., Eglinton, T., Rozanski, K., and Zech, M. (2015). Coupling δ2H and δ18O biomarker results yields information on relative humidity and isotopic composition of precipitation – a climate transect validation study. Biogeosciences *12*, 3913–3924.
Uemura, R., Barkan, E., Abe, O., and Luz, B. (2010). Triple isotope composition of oxygen in atmospheric water vapor. Geophys. Res. Lett. *37*, L04402.
Valley, J.W., Kitchen, N., Kohn, M.J., Niendorf, C.R., and Spicuzza, M.J. (1995). UWG-2, a garnet standard for oxygen isotope ratios: Strategies for high precision and accuracy with laser heating. Geochim. Cosmochim. Acta *59*, 5223–5231.
Wahl, E.R., Diaz, H.F., and Ohlwein, C. (2012). A pollen-based reconstruction of summer temperature in central North America and implications for circulation patterns during medieval times. Glob. Planet. Change *84–85*, 66–74.
Webb, E.A., and Longstaffe, F.J. (2000). The oxygen isotopic compositions of silica phytoliths and plant water in grasses: Implications for the study of paleoclimate. Geochim. Cosmochim. Acta *64*, 767–780.
Webb, E.A., and Longstaffe, F.J. (2002). Climatic influences on the oxygen isotopic composition of biogenic silica in prairie grass. Geochim. Cosmochim. Acta *66*, 1891–1904.
Webb, E.A., and Longstaffe, F.J. (2003). The relationship between phytolith- and plant-water delta O-18 values in grasses. Geochim. Cosmochim. Acta *67*, 1437–1449.
Webb, E.A., and Longstaffe, F.J. (2006). Identifying the δ 18O signature of precipitation in grass cellulose and phytoliths: Refining the paleoclimate model. Geochim. Cosmochim. Acta *70*, 2417–2426.
Welle, B.J.H. ter (1976). On the occurrence of Silica grains in the secondary xylem of the Chrysobalanaceae.
Welp, L.R., Lee, X., Kim, K., Griffis, T.J., Billmark, K.A., and Baker, J.M. (2008). δ18O of water vapour, evapotranspiration and the sites of leaf water evaporation in a soybean canopy. Plant Cell Environ. *31*, 1214–1228.
Wernicke, J., Grießinger, J., Hochreuther, P., and Bräuning, A. (2015). Variability of summer humidity during the past 800 years on the eastern Tibetan Plateau inferred from δ18O of tree-ring cellulose. Clim Past *11*, 327–337.
White, F., Unesco, and Office, U.N.S.-S. (1983). The vegetation of Africa: a descriptive memoir to accompany the Unesco/AETFAT/UNSO vegetation map of Africa (Unesco).

Biogeosciences Discuss., https://doi.org/10.5194/bg-2017-471
Manuscript under review for journal Biogeosciences
Discussion started: 8 November 2017
© Author(s) 2017. CC BY 4.0 License.

882 **Table 1.** Growth chamber experiment : experimental set-up, phytolith content and morphological characteristics, isotope enrichments ($\Delta^{*}_{A\text{-}B} = ({}^{*}\delta_a$
883 $- {}^{*}\delta_b) / ({}^{*}\delta_b / 1000 + 1)$), associated ^{17}O-excess$_e$ (^{17}O-excess$_e$ = ln ($\Delta^{17} + 1$) – 0.528 x ln ($\Delta^{18} + 1$) and θ (θ = ln ($\Delta^{17}{}_{A\text{-}B} + 1$) / ln ($\Delta^{18}{}_{A\text{-}B} + 1$)) values
884 of phytoliths compared to either leaf water or irrigation water and of leaf water compared to irrigation water. Av : average ; n : number of replicates ;
885 SD : standard deviation calculated on the replicates; n.v. : no value. Transp. (l/day), Conc. (% d.w.) and LC (%) stands for transpiration expressed
886 in liter/day, phytolith concentration expressed in % of the dry weight and long cell abundance in the phytolith morphological assemblage expressed
887 in % of counted phytoliths with taxonomic significance, respectively. ^{17}O-excess = ln (δ^{17}O + 1) – 0.528 x ln (δ^{18}O + 1).

Biogeosciences Discuss., https://doi.org/10.5194/bg-2017-471
Manuscript under review for journal Biogeosciences
Discussion started: 8 November 2017
© Author(s) 2017. CC BY 4.0 License.

Experimental set-up								Phytoliths (Phyto)			Leaf water -irrigation water (LW-IW)				Phytolith - leaf water (Phyto-LW)				Phytolith -irrigation water (Phyto-IW)			
Duration	Temp.	SD	RH	SD	Light	Transp.	Biomass	Sample	Conc.	LC	$\Delta^{18}O$	$\Delta^{17}O$	^{17}O-excess$_{st}$	θ	$\Delta^{18}O$	$\Delta^{17}O$	^{17}O-excess$_{st}$	θ	$\Delta^{18}O$	$\Delta^{17}O$	^{17}O-excess$_{st}$	θ
day	°C		%		mmol/m²/sec	l/day	g		% d.w.	%	‰		per meg		‰		per meg		‰		per meg	
11	25	0.2	###	1	278		13	P1-40-29-04-16	n.v.		16.370	8.455	-154	0.519	34.353	17.493	-492	0.513	51.285	26.350	-398	0.520
10	25	0.2	41	1.1	278	0.49	21	P10-40-10-05-16	0.8		13.259	6.823	-155	0.516	33.278	17.430	-5	0.528	47.809	24.595	-361	0.520
11	25	0.4	42	1	311	0.69	37	P1-40-20-05-16	0.8	21	16.479	8.496	-170	0.518	29.262	15.316	-29	0.527	46.992	24.148	-385	0.520
14	25	0.2	41	0.9	278	0.65	38	P1-40-03-06-16	1.8		n.v.	n.v.	n.v.	n.v.	32.142	16.801	-43	0.527	n.v.	n.v.	n.v.	n.v.
					Av.	**0.61**			**1.2**		**15.369**	**7.925**	**-159**	**0.517**	**32.259**	**16.760**	**-142**	**0.524**	**48.695**	**25.031**	**-381**	**0.520**
					SD	**0.11**			**0.6**		**1.829**	**0.955**	**9**	**0.001**	**2.192**	**1.012**	**234**	**0.007**	**2.280**	**1.164**	**19**	**0.000**
11	25	0.5	60	2.5	311		21	P10-60-29-04-16	n.v.		15.230	7.895	-117	0.520	28.858	15.137	2	0.528	45.242	23.343	-288	0.521
11	25	0.2	61	1	289	0.57	33	P2-60-10-05-16	0.7		17.028	8.775	-178	0.517	25.587	13.496	66	0.531	43.689	22.562	-266	0.522
10	25	0.8	60	4.8	311	0.60	48	P10-60-20-05-16	0.8	13	12.087	6.262	-101	0.520	30.061	15.752	-9	0.528	43.175	22.291	-271	0.522
14	25	0.6	60	3.2	311	0.76	60	P10-60-03-06-16	1.3		n.v.	n.v.	n.v.	n.v.	32.833	17.165	-38	0.527	n.v.	n.v.	n.v.	n.v.
					Av.	**0.64**			**0.9**		**14.781**	**7.644**	**-132**	**0.519**	**29.335**	**15.387**	**5**	**0.528**	**44.035**	**22.732**	**-275**	**0.522**
					SD	**0.10**			**0.3**		**2.501**	**1.275**	**41**	**0.001**	**3.002**	**1.520**	**44**	**0.002**	**1.076**	**0.546**	**11**	**0.000**
11	25	0.2	80	2.8	289		24	P2-85-29-04-16	n.v.		7.857	4.076	-65	0.520	27.977	14.652	-23	0.527	36.516	18.912	-201	0.522
10	25	0.2	82	1.3	289	0.28	27	P1-85-10-05-16	0.4		7.989	4.148	-62	0.520	28.209	14.765	-31	0.527	36.898	19.103	-209	0.522
11	25	0.2	77	2.5	278	0.22	27	P2-85-20-05-16	0.6	10	6.702	3.435	-97	0.513	28.636	14.985	-34	0.527	35.979	18.593	-241	0.521
14	25	0.2	83	1.1	289	0.36	37	P2-85-03-06-16	1.0		n.v.	n.v.	n.v.	n.v.	28.864	15.035	-101	0.524	n.v.	n.v.	n.v.	n.v.
					Av.	**0.29**			**0.7**		**7.516**	**3.886**	**-75**	**0.518**	**28.422**	**14.859**	**-47**	**0.526**	**36.464**	**18.869**	**-217**	**0.522**
					SD	**0.07**			**0.3**		**0.708**	**0.392**	**20**	**0.004**	**0.402**	**0.181**	**36**	**0.001**	**0.461**	**0.257**	**21**	**0.001**
11	25		100		307	0.03	31	P3-100-10-05-16	0.0		14.789	7.659	-122	0.520	21.133	11.117	14	0.529	36.663	18.977	-212	0.522
10	25		100		307	0.01		P3-100-20-05-16	0.0	5	7.736	4.023	-54	0.521	27.286	14.269	-46	0.526	35.672	18.467	-208	0.522
14	25		100		307	0.05	21	P3-100-03-06-16	0.2		n.v.	n.v.	n.v.	n.v.	35.424	18.456	-93	0.525	n.v.	n.v.	n.v.	n.v.
					Av.	**0.03**			**0.1**		**11.263**	**5.841**	**-88**	**0.520**	**27.948**	**14.614**	**-42**	**0.527**	**36.167**	**18.722**	**-210**	**0.522**
					SD	**0.02**			**0.1**		**4.987**	**2.571**	**48**	**0.001**	**7.168**	**3.681**	**54**	**0.002**	**0.701**	**0.361**	**3**	**0.000**
								Av.						**0.519(a)**			**-26(b)**	**0.526(a)**				
								SD						**0.002(a)**			**42(b)**	**0.004(a)**				

(a) Calculated on the raw values
(b) Calculated on the raw values without taking into account sample P1-40-29-04-16.

Biogeosciences Discuss., https://doi.org/10.5194/bg-2017-471
Manuscript under review for journal Biogeosciences
Discussion started: 8 November 2017
© Author(s) 2017. CC BY 4.0 License.

Table 2. Natural West and Central African samples: coordinates, climatic parameters, d/p, $\delta^{18}O$, $\delta'^{18}O$, $\delta^{17}O$, $\delta'^{17}O$ and ^{17}O-excess obtained for the phytolith assemblages. Average and standard deviation (SD) are given for replicates. MAP: Mean Annual Precipitation; MAT: Mean Annual Temperature; RH: mean annual relative humidity; RH15: RH at 15:00 H UTC; RH-rd0>1: relative humidity average for months with days with precipitation higher than 0.1mm; RH15-rd0>1: RHrd0>1 at 15:00 H UTC. See text for data source and calculation.

Identifier	Lat	long	MAP	MAT	RH	RH-rd0>1	RH15	RH15-rd0>1	$\delta^{18}O_{hyd}$ (1)	D/P	n	$\delta^{18}O$	SD	$\delta^{17}O$	SD	^{17}O-excess	SD	$\delta^{18}O_{hyto-HW}$	$\Delta^{18}O_{hyto-Pre}$
			mm	°C	%	%	%	%	‰			‰		‰		per meg		‰	
Savana																			
RIM 3	21.5	-13.0	52.4	27.3	47.1	61.7	35.4	47.0	-3.220	0.03		33.681		17.367		-243		2.942	37.020
RIM 8	21.0	-12.2	49.1	28.2	44.1	60.5	33.0	45.9	-3.414	0.04		35.426		18.304		-243		4.843	38.973
MAU06	20.6	-12.6	68.8	27.6	44.0	58.0	33.0	44.1	-3.829	0.04		29.292		15.088		-268		-1.394	33.248
RIM 11	16.9	-15.2	209.1	27.3	45.9	68.5	32.5	52.2	-4.047	0.04		38.218		19.785		-211		7.480	42.437
RIM 10	16.7	-15.2	227.6	27.2	45.7	68.7	32.1	52.1	-4.042	0.01		38.901		20.094		-256		8.142	43.117
S33	16.4	-14.8	270.5	27.7	42.7	57.6	29.7	41.8	-3.861	0.04		36.615		18.939		-225		5.944	40.633
S32	16.3	-15.4	284.4	27.3	46.9	61.6	33.5	46.2	-3.768	0.04		38.001		19.617		-266		7.263	41.927
C4L1	16.1	-14.0	287.7	29.8	40.9	57.1	29.4	42.9	-3.874	0.02	2	35.532	0.368	18.340	0.203	-262	11	5.236	39.559
S40	16.1	-13.9	329.1	29.2	40.6	56.8	29.4	43.0	-3.969	0.06		36.019		18.592		-262		5.613	40.148
S29	16.1	-14.9	313.0	27.8	43.6	59.1	30.8	43.7	-3.833	0.05	2	36.085	0.583	18.653	0.303	-236	0	5.432	40.072
82-46	16.0	-16.0	316.4	27.1	53.0	67.5	40.1	54.2	-3.604	0.03		34.145		17.654		-228		3.374	37.885
82-47	16.0	-16.0	316.4	27.1	53.0	67.5	40.1	54.2	-3.604	0.04		37.101		19.169		-247		6.330	40.851
S44	15.8	-13.5	369.1	29.6	40.2	57.2	29.6	44.1	-4.073	0.04	2	36.875	0.593	19.041	0.284	-258	24	6.544	41.115
C4L3	15.4	-13.7	467.7	29.6	41.2	59.1	30.3	45.7	-4.023	0.05	2	34.262	0.312	17.652	0.175	-290	13	3.924	38.439
S54	15.3	-13.0	443.6	29.7	41.3	60.0	31.0	47.2	-4.009	0.04		36.227		18.680		-282		5.916	40.398
S58	15.1	-12.8	478.6	29.7	42.0	56.3	31.7	44.3	-4.009	0.05	2	36.823	0.234	19.006	0.143	-266	21	6.512	40.997
C5L1	15.0	-12.9	583.2	29.7	42.5	57.2	32.1	44.9	-3.972	0.06	3	29.966	0.483	15.500	0.257	-208	7	-0.346	34.073
83-62	14.9	-12.3	515.8	29.7	42.9	58.1	32.6	46.0	-4.097	0.06	2	36.988	0.747	19.095	0.424	-262	36	6.673	41.254
S5	14.7	-16.2	511.1	28.1	53.3	68.6	39.2	53.9	-3.789	0.08	2	24.595	0.115	12.704	0.064	-205	4	-5.994	28.492
82-79	14.2	-16.1	669.0	28.3	54.2	70.1	39.9	55.2	-3.774	0.03	2	34.494	0.046	17.798	0.076	-229		3.943	38.413
83-75	14.1	-12.7	736.2	29.1	46.7	63.1	35.6	50.3	-3.936	0.03		32.949		16.969		-290		2.533	37.032
82-78	14.1	-16.1	669.0	28.3	55.2	71.0	40.8	56.2	-3.768	0.18		24.075		12.437		-201		-6.477	27.948
S84	13.9	-13.4	775.2	28.9	47.4	64.1	36.1	50.9	-4.040	0.03	2	33.137	0.435	17.080	0.221	-277	5	2.680	37.328
S118	13.6	-13.7	878.1	28.6	49.6	66.3	37.7	52.9	-4.008	0.02		30.462		15.779		-188		-0.046	34.608
S88	13.6	-13.6	880.0	28.6	49.4	66.2	37.7	52.9	-3.996	0.02		28.777		14.900		-189		-1.720	32.904
83-120	13.5	-13.8	934.5	28.5	50.7	67.3	38.7	53.8	-3.984	0.05		32.128		16.570		-262		1.607	36.256
83-122	13.4	-14.9	947.3	28.1	53.6	68.1	39.8	53.7	-3.928	0.03	2	31.733	0.628	16.396	0.335	-231	9	1.143	35.802
S122	13.3	-13.9	934.5	28.5	52.1	68.1	39.7	53.7	-3.971	0.03		34.977		18.095		-219		4.456	39.103
S93	13.3	-13.2	1005.3	28.6	51.6	68.2	39.7	55.1	-3.925	0.08		30.521		15.787		-211		0.022	34.581
83-98	13.1	-12.8	1067.0	28.7	52.7	69.3	40.8	56.3	-4.060	0.04		30.138		15.621		-177		-0.354	34.337
S128	13.0	-14.1	1055.1	28.2	54.7	70.2	41.7	56.5	-3.765	0.07	2	34.665	0.567	17.919	0.265	-233	29	4.094	38.576
S.130	12.9	-14.2	1113.9	28.0	55.1	70.3	41.8	56.4	-3.961	0.03	3	36.562	0.515	18.868	0.254	-268	19	5.952	40.684
83-103	12.9	-12.4	1114.0	28.5	53.7	70.4	41.8	57.5	-4.329	0.03		30.969		15.981		-249		0.446	35.452
S.138	12.9	-14.9	1127.1	27.7	56.8	70.9	42.4	56.6	-4.069	0.03	2	36.471	0.516	18.842	0.273	-247	5	5.800	40.706
S136	12.8	-14.7	1113.4	27.8	57.4	71.5	43.3	57.4	-4.023	0.02		33.987		17.507		-246		3.335	38.163
83-116	12.7	-12.2	1233.2	28.5	54.8	71.4	42.7	58.5	-4.316	0.03	2	31.573		16.280		-264		1.046	36.044
83-115	12.4	-12.3	1301.3	27.8	56.5	66.8	44.2	53.8	-4.170	0.01	2	32.027	0.407	16.554	0.229	-226	17	1.389	36.348
Wooded savanna																			
83-8	14.9	-15.9	485.2	28.0	50.9	67.0	37.3	52.4	-3.948	0.16		37.500		19.352		-270		6.886	41.612
S7	14.8	-16.0	513.6	28.2	52.0	67.9	38.0	53.1	-4.263	0.26		29.931		15.449		-241		-0.637	34.340
83-4	14.7	-16.5	539.7	27.0	57.4	70.9	43.7	57.3	-3.821	0.43		26.472		13.657		-231		-4.310	30.409
82-77	14.6	-16.3	535.5	28.0	53.5	69.0	39.2	54.0	-3.798	0.14	2	35.841	0.761	18.481	0.406	-281	10	5.239	39.790
S91	13.6	-13.4	883.1	28.7	49.4	66.2	37.8	53.0	-3.984	0.40	2	35.115	0.151	18.173	0.109	-213	30	4.623	39.255
C4L8	13.5	-13.7	878.1	28.6	50.7	67.3	38.7	53.8	-3.984	0.13		32.829		16.992		-206		2.322	36.960
83-127	13.1	-14.1	1055.1	28.2	53.6	69.3	40.7	55.5	-3.785	0.49	2	36.280	0.242	18.746	0.125	-244	1	5.709	40.217
Enclosed savanna																			
Biendi 1	-2.0	11.1	1839.0	25.9	80.9	80.9	67.4	67.4	-3.687	0.76		33.640	0.022	17.383	0.032	-205	20	2.651	37.465
Doubou 1	-1.8	10.9	1986.0	25.9	81.2	81.2	67.9	67.9	-3.631	1.58		32.446	0.610	16.805	0.325	-194	8	1.470	36.209
Humid forest																			
83-151	12.5	-16.6	1428.6	26.5	65.8	74.9	51.0	60.8	-3.787	6.78		33.650		17.439		-187		2.778	37.580
S155	12.5	-16.3	1352.6	27.0	64.4	74.3	49.4	59.9	-3.777	4.85	2	29.520	0.181	15.295	0.090	-181	4	-1.269	33.423
04-94		13.1	1676.4	24.3	81.4	81.4	65.8	65.8	-4.464	2.44	2	33.176	0.235	17.240	0.118	-140	4	1.910	37.809
04-88		12.4	1707.0	24.9	81.9	81.9	67.1	67.1	-4.458	5.45		33.692	0.424	17.497	0.202	-151	18	2.534	38.321
04-47	-0.2	12.3	1724.0	26.2	82.1	82.1	67.4	67.4	-1.515	3.48		33.502	0.022	17.364	0.006	-185	17	2.577	35.070
04-66	-0.2	12.5	1690.6	25.8	82.0	82.0	67.3	67.3	-4.354	1.84		30.413	0.624	15.764	0.300	-177	24	-0.586	34.919
04-65	-0.2	12.6	1690.6	25.8	82.0	82.0	67.3	67.3	-4.195	2.19		33.334	0.591	17.306	0.281	-156	25	2.336	37.687
04-118	-0.2	10.5	2148.4	26.4	82.5	82.5	69.2	69.2	-3.556	3.69		32.352	0.393	16.787	0.200	-164	4	1.458	36.036
Dimonika	-4.1	12.4	1286.6	24.7	80.3	80.3	68.1	68.1	-4.284	5.80		31.412		16.254		-205		0.208	35.849
Outliers																			
RIM1	16.7	-16.0	216.4	26.7	52.3	72.2	39.4	58.6	-3.857	0.06		38.867		20.026		-305		8.027	42.889
C3L4	15.6	-14.2	362.0	29.3	41.8	59.1	30.3	45.0	-3.968	0.06		25.505	0.170	13.228	0.088	-157	10	-4.877	29.590

(1) Amount weighted average for months with at least one day with precipitation>0.1mm

© Author(s) 2017. CC BY 4.0 License.

898 **Figure captions**
899
900 **Figure 1.** Growth chamber experiment: a) ^{17}O-excess *vs* relative humidity (RH) of irrigation
901 water (IW), soil water (SW), leaf water (LW) and phytolith (Phyto). Error bars show standard
902 deviation (SD) on the replicates. They are smaller than the symbol when not shown. b) ^{18}O-
903 enrichment from irrigation water to leaf water ($^{18}\Delta_{LW\text{-}IW}$), from irrigation water to phytolith
904 ($^{18}\Delta_{Phyto\text{-}IW}$) and from leaf water to phytolith ($^{18}\Delta_{Phyto\text{-}LW}$). c) ^{17}O-excess associated with the
905 enrichment from irrigation water to leaf water ($^{17}O\text{–}excess_{e\ LW\text{-}IW}$), from irrigation water to
906 phytolith ($^{17}O\text{–}excess_{e\ Phyto\text{-}IW}$), and from leaf water to phytolith ($^{17}O\text{–}excess_{e\ Phyto\text{-}LW}$).

907 **Figure 2.** Growth chamber experiment: phytolith types extracted from *Festuca arundinaceae*
908 and observed in natural light microscopy: epidermal long cell (LC), epidermal short cell (SC).

909 **Figure 3.** Natural West and Central African transect: $\boldsymbol{\delta}^{18}O$ of phytoliths ($\boldsymbol{\delta}^{18}O_{Phyto}$) *vs* relative
910 humidity RH-rd0>1 (see fig. 4 for explanation). Error bars show standard deviation (SD) on the
911 replicates. When not shown, they are smaller than the symbol. For comparison, the $\boldsymbol{\Delta}^{18}O_{Phyto\text{-}IW}$
912 *vs* RH line is plotted for comparison.

913 **Figure 4.** Natural West and Central African transect: ^{17}O-excess *vs* relative humidity (RH) of
914 phytolith assemblages from soil tops collected under savanna, wooded savanna, humid forest
915 and enclosed savanna along a humidity gradient (Table 1). The growth chamber $^{17}O\text{–}excess_{e}$
916 $_{Phyto\text{-}IW}$ *vs* RH correlation line is displayed for comparison. a) RH-Av: yearly average of monthly
917 means; b) RH-rd0>1: yearly average of monthly means for months with at least one day with
918 precipitation higher than 0.1mm; c) RH15: RH at 15:00 H UTC; d) RH15-rd0>1: RH-rd0>1 at
919 15:00 H UTC.

920 **Figure 5.** Natural West and Central African transect: ^{17}O-excess of phytoliths ($^{17}O\text{-}excess_{Phyto}$)
921 *vs* d/p.

922 **Figure 6.** Growth chamber experiment: ^{17}O-excess *vs* δ'^{18}O of irrigation water (IW), soil water
923 (SW), leaf water (LW) and phytolith (Phyto). Error bars show standard deviation (SD) on the
924 replicates. They are smaller than the symbol when not shown. The observed bulk leaf water
925 line reflecting $\theta_{LW\text{-}IW}$ = 0.519, the expected phytolith line in agreement with phytoliths
926 polymerizing from the bulk leaf water, and the observed phytolith line are displayed. See text
927 for explanation.

Biogeosciences Discuss., https://doi.org/10.5194/bg-2017-471
Manuscript under review for journal Biogeosciences
Discussion started: 8 November 2017
© Author(s) 2017. CC BY 4.0 License.

928 **Figure 1**

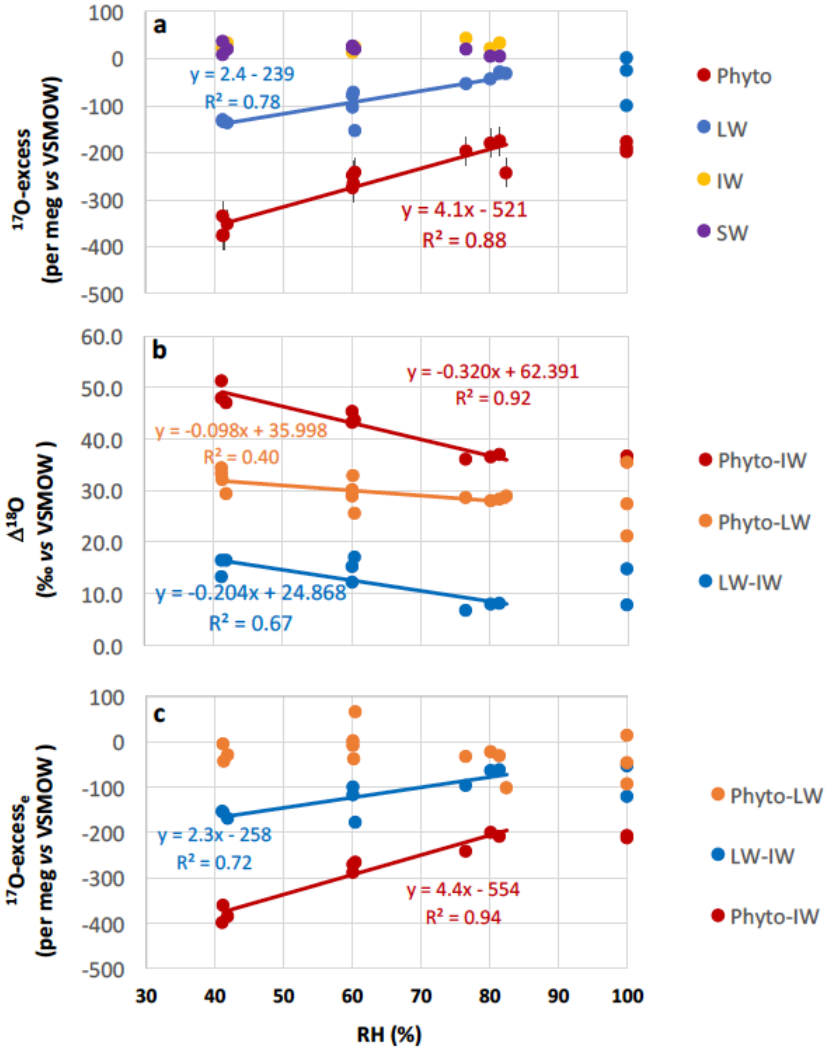

929

Biogeosciences Discuss., https://doi.org/10.5194/bg-2017-471
Manuscript under review for journal Biogeosciences
Discussion started: 8 November 2017
© Author(s) 2017. CC BY 4.0 License.

930 **Figure 2**

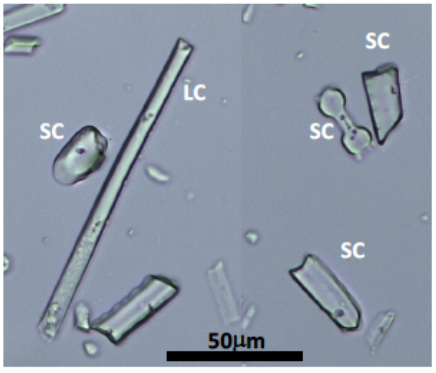

931

Biogeosciences Discuss., https://doi.org/10.5194/bg-2017-471
Manuscript under review for journal Biogeosciences
Discussion started: 8 November 2017
© Author(s) 2017. CC BY 4.0 License.

932 **Figure 3**

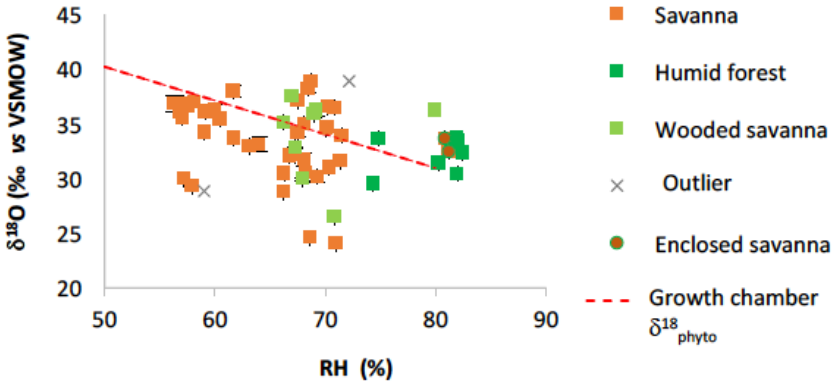

933

Biogeosciences Discuss., https://doi.org/10.5194/bg-2017-471
Manuscript under review for journal Biogeosciences
Discussion started: 8 November 2017
© Author(s) 2017. CC BY 4.0 License.

934 **Figure 4**

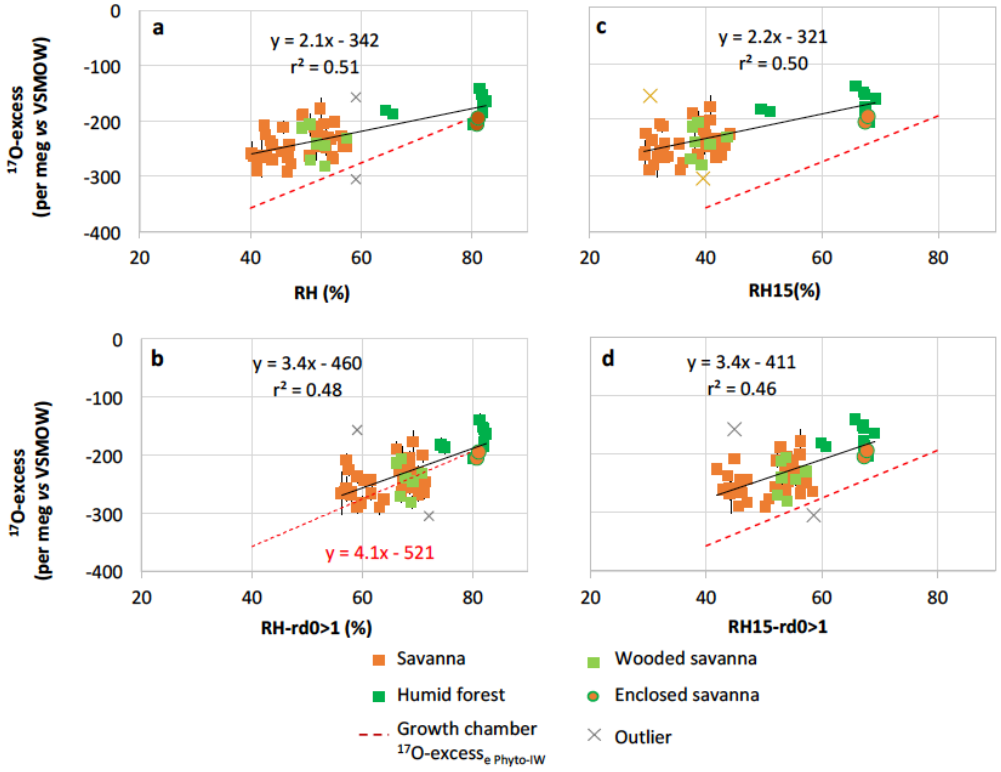

935

Biogeosciences Discuss., https://doi.org/10.5194/bg-2017-471
Manuscript under review for journal Biogeosciences
Discussion started: 8 November 2017
© Author(s) 2017. CC BY 4.0 License.

936 **Figure 5**

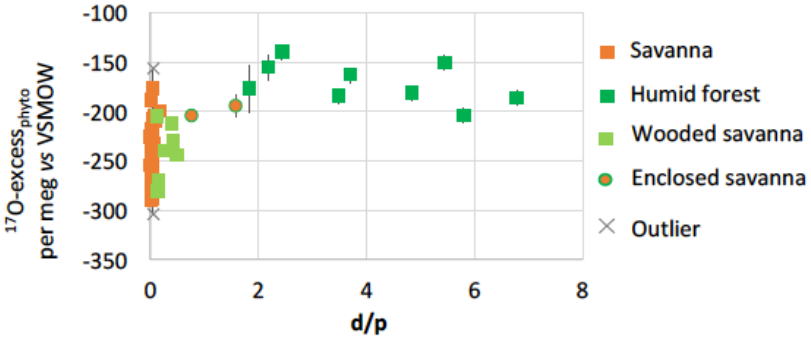

937

Biogeosciences Discuss., https://doi.org/10.5194/bg-2017-471
Manuscript under review for journal Biogeosciences
Discussion started: 8 November 2017
© Author(s) 2017. CC BY 4.0 License.

938 **Figure 6**

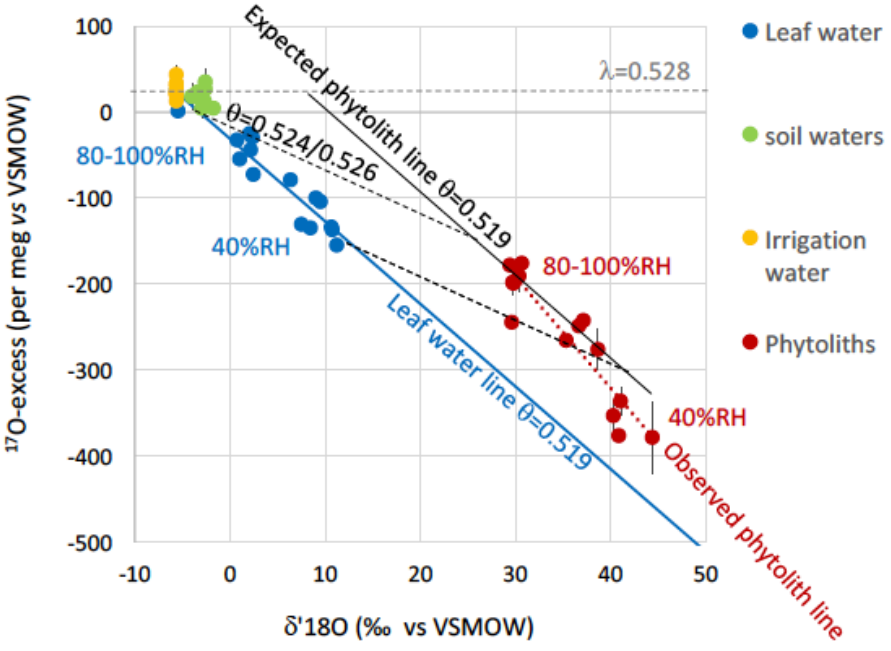

939